

ROSAT observations of the IC 4329A galaxy group^{*}

A.M. Read and W. Pietsch

Max-Planck-Institut für extraterrestrische Physik, Gießenbachstraße, D-85748 Garching, Germany

Received 27 April 1998 / Accepted 13 May 1998

Abstract. We report here the results of high-resolution and spectral imaging X-ray observations, with both the *ROSAT* HRI and PSPC, of the field surrounding the nearby ($D = 64$ Mpc) type 1 Seyfert galaxy IC 4329A and its giant lenticular companion IC 4329. Many point sources are detected, the brightest being associated with IC 4329A itself, having an extremely bright X-ray luminosity of 6×10^{43} erg s⁻¹, and spectral properties compatible with a single power-law model ($\Gamma = 1.73$), with a spectral break at 0.7 keV. Two other bright sources are detected associated with the companion galaxy IC 4329, and a likely quasar 14' to the south-west. We have also established, through optical observations taken at the European Southern Observatory, that three further X-ray point sources, intriguingly positioned with respect to IC 4329A, are in fact nothing to do with the system, and are merely foreground and background objects.

In addition to point source emission, residual, unresolved emission is detected surrounding the IC 4329A/ IC 4329 pair, extending for some 200 kpc. This emission appears markedly two-component, comprising of a spectrally hard and smooth component, circularly-distributed about the central galaxy pair, and a spectrally soft, more clumpy component, positioned almost entirely to the south-east of IC 4329A. The hard component of the residual emission itself appears two-component, one component being due to the 'wings' of the intensely bright IC 4329A source, the other, apparently due to hot (~ 1.5 keV) gas, likely associated with the galaxy group of which IC 4329A and IC 4329 are members. The soft component of the residual emission may be a larger version of the superwinds seen around some ultraluminous far-infrared galaxies, or may even represent a 'stripped wake' of intragroup gas. Evidence for shocked gas due to the central IC 4329A/ IC4329 interaction is also found between the two central galaxies.

Key words: galaxies: individual: IC 4329A – galaxies: interactions – intergalactic medium – galaxies: Seyfert – X-rays: galaxies

1. Introduction

IC 4329A is a nearby ($z = 0.01605$), edge-on, S0, type 1 Seyfert galaxy, at a distance of 64 Mpc ($H_0 = 75$ km s⁻¹ Mpc⁻¹), situated very close to the centre of Abell cluster A3574. This is unusual given that Seyfert galaxies, like most spirals, are rarely found inside clusters (e.g. Osterbrock 1991). This cluster, first described by Shapley (1936), is often referred to as the IC 4329 cluster or group, after its brightest member (e.g. de Vaucouleurs et al. 1964), or as Klemola 27 (Klemola 1969), and is the easternmost and most distant member of the chainlike Hydra-Centaurus Supercluster (Chincarini & Rood 1979).

The heavily reddened type 1 Seyfert nucleus observed within IC 4329A (Winkler et al. 1992) is a strong FIR/X-ray source, the $25\mu\text{m}$ peak in the *IRAS* flux density, suggestive of there being hot gas close to the nucleus. It has the steepest Balmer decrement ($H\alpha/H\beta \simeq 12$) of any known Seyfert, a very steep optical spectral index ($\alpha = 4.4$), and it is seen to show NaI in absorption (Penston & Wilson 1979). Although calculated extinction values indicate that the absolute visual magnitude M_v , is at least -23, and may be as high as -25, IC 4329A appears optically, to be a largely undisturbed edge-on system, with a prominent dust lane.

The brightest galaxy within the cluster, the giant lenticular IC 4329 has a redshift close to that of IC 4329A ($\Delta v = 460$ km s⁻¹), and lies at a projected distance of 59 kpc to the west. As pointed out by Kollatschny & Fricke (1989), these two systems appear to be part of a loose group of seven galaxies, indicating that a number of the group member's activity may well be linked to past interactions. The fact that IC 4329 is a shell galaxy, together with the fact low surface brightness features are observed around IC 4329A (Wolstencroft et al. 1995), suggest that an interaction is taking place between IC 4329 and IC 4329A. Of the seven group members, only IC 4329A shows any indication of significant nuclear activity.

Further evidence for possibly interaction-induced activity is also apparent from emission-line imaging studies. A halo of emission-line gas can be seen around IC 4329A in the $H\alpha$ + $[\text{NII}]$ image of Colbert et al. (1996), extending along the minor axis, $\sim 10''$ (3 kpc) on both sides of the nucleus, with a luminosity of $\sim 2.5 \times 10^{39}$ erg s⁻¹. An almost identical image is seen in Mulchaey et al. (1996). This $H\alpha$ halo is believed by

Send offprint requests to: A.M. Read, (aread@mpe.mpg.de)

^{*} Based partially on observations collected at the European Southern Observatory, La Silla, Chile

both sets of authors to represent an outflow from the nucleus, perhaps a superwind of the type commonly seen in edge-on infrared-luminous galaxies (e.g. McCarthy et al. 1987; Armus et al. 1990).

Radio mapping of the IC 4329A system has brought about some very interesting results also. In a Molonglo Synthesis Telescope (MOST) 843 MHz survey of radio sources in southern Abell clusters, IC 4329A is seen to possess an apparent radio tail $\sim 6'$ long (Unwin 1993), corresponding to a linear size of 110 kpc. This feature implies a radio structure larger than any other known Seyfert, though it must be stressed that the resolution of the MOST observations make it impossible to be certain whether the observed feature is associated with the galaxy or not. Other significant radio observations include those of Unger et al. (1987) at 1490 MHz (and 4860 MHz), where, besides a bright core being visible, an extended region of emission is observed extending $\sim 6''$ towards IC 4329. This feature may well be associated with the interaction. Furthermore, Blank & Norris (1994), in a $4''$ resolution 2.3 GHz observation, observed two $10''$ extensions emanating from the nucleus. The first is roughly in the same direction as the extension seen by Unger et al. (1987). The second, extending to the south-east, perpendicular to the dust-lane of the galaxy, may, according to Blank & Norris (1994), be due to a superwind, driven from the nucleus. Baum et al. (1993) found that the kpc-scale radio emission seen in several Seyfert galaxies tended to align itself with the systems' minor axes, and they concluded that circumnuclear starbursts are the most likely cause.

1.1. Previous X-ray observations

X-ray emission associated with IC 4329A was first suspected when Ariel V detected the steady source 2A 1347-300 (Cooke et al. 1978). The error box however, contained IC 4329 as well, and it was only later (Delvaile 1978) that the source was identified with IC 4329A. Further observations were performed by HEAO 1, both in scanning (Piccinotti et al. 1982) and pointed modes (Tennant & Mushotzky 1983; Mushotzky 1984), and by HEAO 2 (Petre et al. 1984). IC 4329A and IC 4329 also appear in Fabbiano et al.'s (1992) X-ray catalog and atlas.

IC 4329A has also been observed (Miyoshi et al. 1988) with gas scintillation proportional counters aboard the Japanese satellite Tenma (Tanaka 1984). It had been established prior to this that large amplitude variabilities in the X-ray flux are rare within Seyfert galaxies on timescales of seconds to years (Mushotzky 1984), and indeed, no significant change in flux or spectral shape was seen over the six day Tenma observation. The spectral shape above 15 keV however, an almost flat, rather positively-sloped tail (rare for Seyfert 1 galaxies), appeared to be very different when compared to the HEAO 1 data (Mushotzky 1984). Observations of IC 4329A with *Ginga* (Piro et al. 1990) showed a hard X-ray bump above 8 keV, probably produced by absorption or reflection of the central emission by a very thick cold medium close to the nucleus, an idea supported by the detection of 6.4 keV fluorescence lines.

The *ROSAT* PSPC data from IC 4329A have been published recently in conjunction with the *COMPTON GRO* observations (Madejski et al. 1995, hereafter M95), their main result being that IC 4329A's spectrum is compatible with a single power law, of energy spectral index 1, modified by absorption and reflection extending from soft X-rays to γ -rays. What evidence there is of a γ -ray spectral break is weak, and in any case, the energy of this possible break is both higher than that of NGC 4151 (Zdziarski et al. 1993), and higher than that of typical Seyfert 1s (Fabian et al. 1993). The *ROSAT* spectrum of IC 4329 was also presented, it being well described by an optically thin thermal plasma with $kT = 0.9$ keV. As far as the spatial structure obtained with the PSPC is concerned, M95 describe IC 4329A's X-ray source as being consistent with point-like.

Lastly, *ASCA* observations of IC 4329A (Cappi et al. 1996) indicate that the 0.4–10 keV spectrum is best described by a steep power law spectrum passing through a warm absorber, together with a strong reflection component and Fe K line, confirming both the above *ROSAT-GRO* (M95) and separate *ASCA* (Mushotzky et al. 1995) results. Furthermore, as concluded by M95, cold absorption in excess of the Galactic value is required by the data, consistent with the edge-on nature of the galactic disc.

The *ROSAT* X-ray telescope (XRT), with the Position Sensitive Proportional Counter (PSPC) (Pfeffermann et al. 1986) at its focal plane, offers three very important improvements over previous X-ray imaging instruments (such as the *Einstein* IPC). Firstly, the spatial resolution is very much improved, the 90% enclosed energy radius at 1 keV being $27''$ (Hasinger et al. 1992). Secondly, the PSPC's spectral resolution is very much better ($\Delta E/E \sim 0.4$ FWHM at 1 keV) than earlier X-ray imaging instruments, allowing the derivation of characteristic source and diffuse emission temperatures. Lastly, the PSPC internal background is very low ($\sim 3 \times 10^{-5}$ ct s $^{-1}$ arcmin $^{-2}$; Snowden et al. 1994), thus allowing the mapping of low surface brightness emission. The High Resolution Imager (HRI) on the other hand, because of its excellent spatial resolution (more like $5''$) and relative insensitivity to diffuse emission, is an ideal instrument for further investigation into the point source populations (see Trümper (1992) for a description of the *ROSAT* satellite and instruments).

Here we report the results of a 15.5 ks *ROSAT* High Resolution Imager (HRI) observation that addresses one essential aspect of the X-ray emission from IC 4329A and its neighbours that has not been possible until now – that of the high resolution spatial properties of the X-ray emission. Although, as mentioned above, some aspects of the PSPC data have been published (M95), the authors concentrate almost entirely on the spectral properties of the individual systems, and no discussion of the spatial properties is given. We have therefore performed a thorough reanalysis of the 8.3 ks of *ROSAT* PSPC data, concentrating on the spatial properties and on the existence of any extended features. These results are also presented here.

The plan of the paper is as follows. Sect. 2 describes the observation and the preliminary data reduction methods used, Sect. 3 discusses the results as regards the point source emission,

Sect. 4 discusses the results as regards the remaining unresolved emission, and finally a summary is presented in Sect. 5.

2. ROSAT observations and preliminary analysis

2.1. HRI data

The field surrounding IC 4329A was observed with the *ROSAT* HRI on the 14th of January 1995 in essentially two separate observations for a total 15.5 ks. The data appeared essentially very clean, and only 200 seconds of data were removed on the basis of very high ($> 20 \text{ ct s}^{-1}$) and very low ($< 1 \text{ ct s}^{-1}$) count rates, and on large values of atomic oxygen column density along the line of sight.

Source detection and position determination were performed over the full field of view ($\sim 37'$ diameter) with the EXSAS local detect, map detect, and maximum likelihood algorithms (Zimmermann et al. 1992). Images of pixel size $5''$ were used for the source detection. During the source detection procedure, only events detected in the raw HRI channels 2–8 were used, thus reducing the UV/cosmic ray background.

Sources accepted as detections were those with a likelihood $L \geq 8$, and this gave rise to a number of sources. Probabilities P , are related to maximum likelihood values L , by the relation $P = 1 - e^{-L}$. Thus a likelihood L of 8 corresponds to a Gaussian significance of 3.6σ (Cruddace et al. 1988; Zimmermann et al. 1994). The source searching algorithms had difficulty in reliably detecting sources close to the bright central feature. Sources that were ‘detected’ here generally appeared to be extended (i.e. they had a large value of extension likelihood), while possessing only a small number of counts. This is very suggestive of them being merely spurious features situated in the wings of the bright central feature. These sources were excluded from the analysis, leaving the 17 listed in Table 1.

In an effort to improve the accuracy of the HRI source positions, the RA and Dec of five bright sources (H2, H7, H15, H16 and H17) were compared with the APM finding charts of Irwin et al. (1994). The sources associated with the two central galaxies IC 4329A (H11) and IC 4329 (H5), although they appeared to be very coincident, were not used in the re-aligning process, because of the extended nature of both their optical and X-ray emission. A very small offset of $0.10''$ in right ascension and $2.1''$ in declination is observed.

Table 1 lists the 17 detected HRI sources as follows: source number (column 1, prefixed by a ‘H’ to distinguish from PSPC-detected sources, see Sect. 2.2), corrected right ascension and declination (columns 2 and 3), error on the source position (column 4, including a $3.9''$ systematic attitude solution error), likelihood of existence (column 5), net counts and error (column 6) count rates and errors after applying deadtime and vignetting corrections (column 7), and $0.1 - 2.4 \text{ keV}$ flux, assuming a 5 keV thermal bremsstrahlung model (column 8). Count rates of the HRI-detected point sources can be converted into fluxes (and into luminosities), assuming other additional spectral models, e.g. thermal bremsstrahlung and Raymond & Smith hot plasma models (with cosmic abundances) at temperatures of 0.3 keV

and 3.0 keV . HRI Conversion factors (in units of $10^{-11} \text{ erg cm}^{-2} \text{ cts}^{-1} \text{ s}^{-1}$) for these models, from count rate (in s^{-1}) into flux (corrected for Galactic absorption), are as follows: Thermal bremsstrahlung: 11.4 (0.3 keV) and 5.3 (3.0 keV); Raymond & Smith hot plasma: 11.0 (0.3 keV) and 5.2 (3.0 keV). As a final point, only source H5 is flagged as extended (at a likelihood of 173), with a FWHM of $12.4''$.

Fig. 1 shows the inner 25×25 arcminute field of view (where all of the 17 sources listed in Table 1 are visible). Sources coincident with both IC 4329A (H11, with sources H9, H10, H12 and H13 in close proximity) and IC 4329 (H5) are visible, as is a further bright source (H1), $15'$ to the southwest of IC 4329A.

To investigate whether any residual, low surface brightness emission is visible, an adaptive filtering technique was used to create an intensity-dependent smoothed image. The signal-to-noise level of low surface brightness emission is boosted by smoothing lower and lower intensity sections of the image using Gaussians of progressively larger FWHM. Photons (again, from raw channels 2–8) were binned into an image of pixel size $8''$. Pixels of amplitude 1 (2,3,4,5,6,7,8) were smoothed with a Gaussian of FWHM $170''$ (120,85,60,40,30,20,15)'. Pixels of amplitude greater than 8 remained unsmoothed, thus ensuring that the bright point sources were not smoothed into the background regions. The resultant image is shown as a contour map overlaid on an optical image in Fig. 2 (the optical image is taken from the U.K. Schmidt plate digitised sky survey).

2.2. PSPC data

The field surrounding IC 4329A was observed with the *ROSAT* PSPC for a total of 8.23 ks, in five separate observation intervals between the 12th and the 14th of January 1993.

Source detection and position determination were performed over the full field of view as with the HRI data, using the EXSAS local detect, map detect, and maximum likelihood algorithms (Zimmermann et al. 1992). As with the HRI analysis, it is very doubtful whether many of the sources initially detected close to the bright central source, associated with IC 4329A, are true detections. Again, as with the HRI, those sources close to the bright central source with a large value of extension likelihood and a low number of counts were excluded from the analysis, leaving 22 sources.

As with the HRI analysis, an effort was made to correct the attitude solution. Comparisons were made between the positions of 4 bright point sources (P3, P11, P12, P14) and the APM finding charts (Irwin et al. 1994). The positions of the bright sources associated with the central galaxies were not used in the re-aligning, on account of their extended nature. An offset (purely in the north-south direction) of $7''$ is seen.

22 sources were detected with a likelihood $L \geq 10$ over the entire PSPC field of view. The 17 sources detected within the central $30' \times 30'$ area are listed below in Table 2 as follows: source number (column 1, prefixed by a ‘P’ for PSPC), corrected right ascension and declination (columns 2, 3), error on the source position (column 4, including a $3.9''$ systematic attitude solution error), likelihood of existence (column 5), net

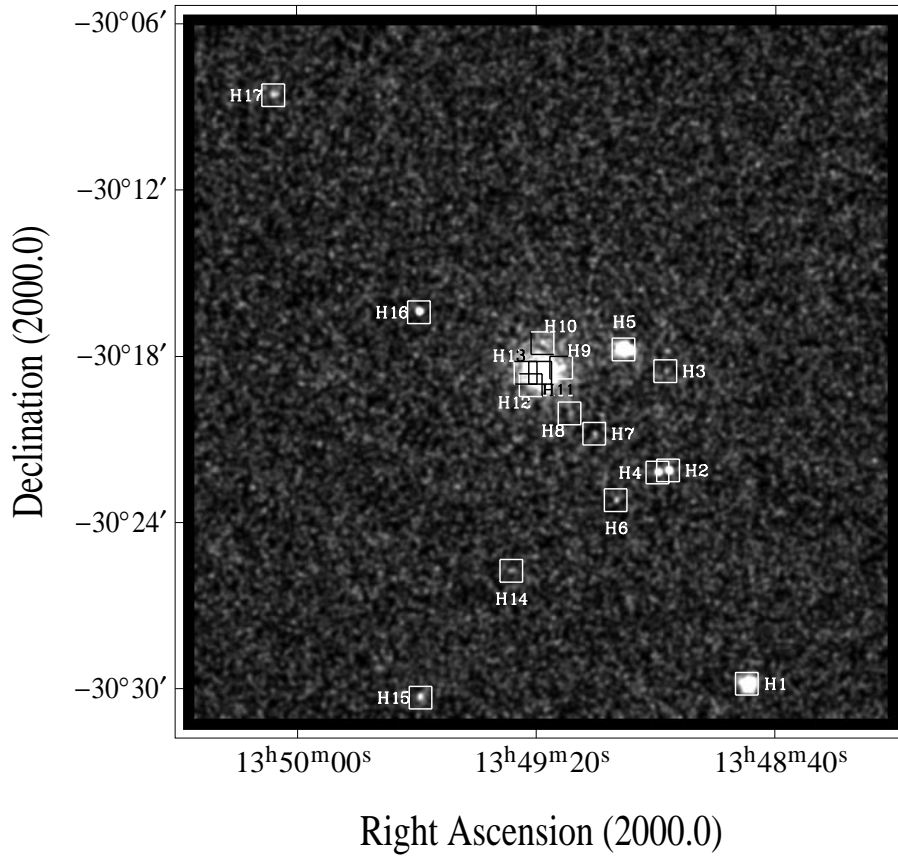


Fig. 1. Grey-scale image of the X-ray flux seen with the *ROSAT* HRI over the central $25 \times 25'$ field. The image was constructed with a pixel size of $2''$, and smoothed with a Gaussian of FWHM $10''$. The point sources, as given in Table 1, are enclosed by boxes and numbered.

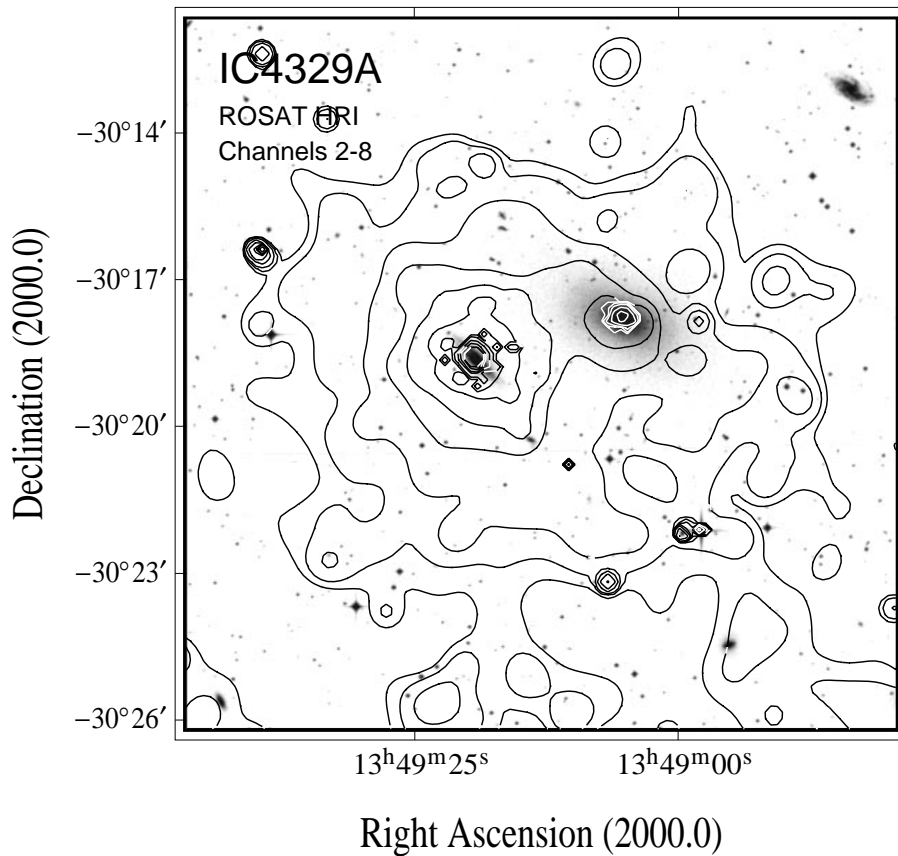


Fig. 2. *ROSAT* HRI map of the IC 4329A field obtained using an adaptive filtering technique (see text), overlaid on a digitized sky survey image. Only channels 2–8 are used. The contour levels are at 2, 3, 5, 9, 15, 31, 63, 127, 255, 511, 1023 and 2047σ (σ being 1.0×10^{-3} cts s^{-1} arcmin^{-2}) above the background (12.9×10^{-3} cts s^{-1} arcmin^{-2}).

Table 1. X-ray properties of point sources detected with the HRI (see text). Tabulated fluxes assume a 5 keV thermal bremsstrahlung model and a hydrogen column density of $N_{\text{H}} = 4.4 \times 10^{20} \text{ cm}^{-2}$ (see text for conversion factors for different temperatures/models).

Source	R.A. (J2000) (^h ^m ^s)	Dec. (J2000) ([°] ['] ^{''})	R_{err} (^{''})	Lik.	Net counts	Count rate (10^{-4} s^{-1})	F_{x} ($10^{-14} \frac{\text{erg}}{\text{cm}^2 \text{s}}$)
(1)	(2)	(3)	(4)	(5)	(6)	(7)	(8)
H1	13 48 44.5	-30 29 47	4.6	354.3	256.4±17.4	183.2±12.4	95.4±6.5
H2	13 48 57.8	-30 22 05	4.2	128.6	58.8±8.0	39.6±5.4	20.6±2.9
H3	13 48 58.2	-30 18 30	5.5	8.4	7.6±3.2	5.1±2.1	2.7±1.1
H4	13 48 59.5	-30 22 10	4.3	81.4	45.1±7.2	30.3±4.8	15.8±2.5
H5	13 49 05.2	-30 17 43	4.1	314.2	323.7±19.3	215.7±12.9	112.3±6.6
H6	13 49 06.5	-30 23 10	5.0	15.0	13.8±4.2	9.3±2.8	4.9±1.5
H7	13 49 10.1	-30 20 46	4.8	13.2	9.9±3.4	6.6±2.3	3.4±1.2
H8	13 49 14.3	-30 20 02	5.3	8.6	8.4±3.4	5.6±2.2	2.9±1.2
H9	13 49 15.7	-30 18 23	8.1	14.8	22.1±5.8	14.7±3.8	7.7±2.0
H10	13 49 18.8	-30 17 30	8.2	11.1	16.1±5.0	10.7±3.3	5.6±1.7
H11	13 49 19.2	-30 18 34	3.9	23751.3	10577.9±103.1	7003.2±68.3	3645.0±35.6
H12	13 49 20.9	-30 19 01	8.6	12.8	28.9±6.8	19.1±4.5	9.9±2.3
H13	13 49 21.6	-30 18 34	9.7	10.3	30.3±7.2	20.0±4.8	10.4±2.5
H14	13 49 24.0	-30 25 43	6.3	8.8	10.2±3.8	6.9±2.6	3.6±1.4
H15	13 49 39.2	-30 30 17	8.1	26.5	39.7±8.0	28.0±5.6	14.6±3.0
H16	13 49 39.4	-30 16 23	4.2	108.4	46.0±7.6	35.1±5.1	18.2±2.7
H17	13 50 03.7	-30 08 33	11.3	21.2	46.0±9.5	33.1±6.8	17.2±3.5

counts and error (column 6) count rates and errors after applying deadtime and vignetting corrections (column 7), and the (0.1–2.4 keV) flux, assuming a 5 keV thermal bremsstrahlung model (column 8). The only source flagged as extended is P6 (corresponding to HRI source H5; see Table 1), at a likelihood of 186, and with a FWHM of 45.8''.

Fig. 3 shows a broad band (channels 8–235, corresponding approximately to 0.08–2.35 keV) contour image of the central region close to the centre of the field of view. All of the sources listed in Table 2 are visible including sources associated with both IC 4329A (P8) and IC 4329 (P6). Also shown in Fig. 3 are three smaller images, again showing the central emission, selected over three separate spectral bands – the ‘soft’ band (channels 8–41), the ‘hard 1’ band (channels 52–90) and the ‘hard 2’ band (channels 91–201).

Comparison of Fig. 3 with Fig. 1 shows many sources visible in both the HRI and in the PSPC fields of view. Of the 9 HRI sources with a high value (> 15) of detection likelihood, *every one* has a PSPC counterpart. The converse is also true; *all* 8 of the PSPC sources with detection likelihoods greater than 27 (that lie within the HRI field of view), have a HRI counterpart. We can be very confident therefore, that all of these features are genuine point sources. The joint HRI/PSPC properties of these bright sources, that we concentrate on below, are summarised in Table 3 as follows: HRI source number (column 1), PSPC source number (column 2), offset (in arcsec) between the (attitude-corrected) HRI and PSPC positions (column 3), count rates and errors, after applying deadtime and vignetting corrections, for the HRI (column 4), the PSPC (column 5), and the PSPC analysis of M95 (column 6, - note that a different technique has been used here - see M95). Fluxes, corrected for

Galactic absorption, are given in column 7 (HRI) and column 8 (PSPC) assuming in both cases a 5 keV thermal bremsstrahlung spectrum. It may appear that some discrepancy exists between the PSPC- and HRI-calculated fluxes, especially in the brighter sources. This could be due either to time variability (discussed in the next section) or to the assumption of the wrong spectral model (discussed in Sect. 3). The final column (column 9) of Table 3 gives the nearest bright optical counterpart, using the APM finding charts of Irwin et al. (1994); type (S–stellar, G–galaxy, F–faint), B magnitude, and offset (from the HRI position) in arcsec.

2.3. Time variability study of point sources

A time variability study was performed for all of the sources detected in either the ROSAT HRI and PSPC fields of view, with special attention paid to the nine brightest sources (eight in the PSPC - see above) detected with both instruments.

For the HRI-detected sources, the complete observation was binned into five observation blocks (of between 2 and 4 ks). A maximum likelihood search at the source positions given in Table 1 was performed for each of the five observation blocks, the vignetting and deadtime corrected count rates (and errors) calculated within a cut radius of $1.5 \times$ the PSF FWHM at the source positions. Where a source was not detected with a likelihood $L > 3.1$ (corresponding to a Gaussian significance of 2σ), a 2σ upper limit to the count rate was calculated. An essentially identical procedure was followed for the PSPC data, the observation binned again into five observation blocks (of ~ 1.6 ks each). A cut radius of $2.5 \times$ the PSF FWHM was used. For the very bright source IC 4329A, the timing analyses de-

Table 2. X-ray properties of point sources detected with the PSPC (see text). Tabulated fluxes assume a 5 keV thermal bremsstrahlung model and a hydrogen column density of $N_{\text{H}} = 4.4 \times 10^{20} \text{ cm}^{-2}$ (see text for conversion factors for different temperatures/models).

Source	R.A. (J2000) (^h ^m ^s)	Dec. (J2000) ([°] ['] ^{''})	R_{err} (^{''})	Lik.	Net counts	Count rate (10^{-3} s^{-1})	F_{x} ($10^{-14} \frac{\text{erg}}{\text{cm}^2 \text{ s}}$)
(1)	(2)	(3)	(4)	(5)	(6)	(7)	(8)
P1	13 48 37.0	-30 13 10	12.3	20.2	26.6±6.5	3.4±0.8	6.3±1.5
P2	13 48 42.9	-30 13 13	16.3	12.6	18.1±5.6	2.3±0.7	4.3±1.3
P3	13 48 44.9	-30 29 42	4.6	1767.4	697.6±27.3	94.2±3.7	175.6±6.9
P4	13 48 58.6	-30 22 07	6.9	151.9	111.4±11.7	14.1±1.5	26.3±2.8
P5	13 49 03.0	-30 19 35	19.1	18.7	42.9±8.9	5.4±1.1	10.1±2.1
P6	13 49 05.6	-30 17 46	5.1	1273.4	647.2±26.7	81.4±3.4	151.7±6.3
P7	13 49 07.0	-30 22 58	8.8	37.7	35.4±7.0	4.5±0.9	8.4±1.7
P8	13 49 19.4	-30 18 36	3.9	26484.9	21889.8±352.2	2746.4±44.2	5118.3±82.4
P9	13 49 28.6	-30 17 39	15.4	16.1	29.4±7.0	3.7±0.9	6.9±1.7
P10	13 49 30.4	-30 18 43	14.8	10.1	16.7±5.4	2.1±0.7	3.9±1.3
P11	13 49 38.9	-30 30 14	12.9	29.7	39.7±7.8	5.3±1.0	9.9±1.9
P12	13 49 39.4	-30 16 22	6.1	158.3	100.0±10.9	12.7±1.4	23.7±2.6
P13	13 49 56.5	-30 10 30	17.3	10.4	17.8±5.6	2.4±0.7	4.5±1.3
P14	13 50 04.0	-30 08 39	10.4	58.2	60.2±9.1	8.2±1.2	15.3±2.2
P15	13 50 18.0	-30 07 54	21.5	13.1	25.7±6.9	3.6±1.0	6.7±1.9
P16	13 50 18.7	-30 26 06	15.9	21.6	35.1±7.7	4.8±1.1	8.9±2.1
P17	13 50 30.7	-30 10 43	23.7	11.8	25.8±7.2	3.7±1.0	6.9±1.9

Table 3. X-ray properties of point sources detected with both the HRI and the PSPC (see text). Tabulated fluxes for both the HRI and PSPC assume a 5 keV thermal bremsstrahlung spectrum, assuming a hydrogen column density of $N_{\text{H}} = 4.4 \times 10^{20} \text{ cm}^{-2}$. Note that for H1-P3, H5-P6 and H11-P8, further detailed spectral analysis has been performed (see Sect. 3). Note also that the PSPC source P4 is resolved by the HRI into two separate sources, H2 and H4.

HRI ident.	PSPC ident.	sep. (^{''})	Count rate (10^{-3} s^{-1})			F_{x} ($10^{-14} \text{ erg cm}^{-2} \text{ s}^{-1}$)		Identification
(1)	(2)	(3)	(HRI)	(PSPC)	(PSPC; M95)	(HRI)	(PSPC)	(9)
H1	P3	7.2	18.3±1.2	94.2±3.7	86.0±6.0	95.4±6.5	175.6±6.9	S (16.5) 2.9 ^{''}
H2	P4	10.6	3.9±0.5	14.1±1.5		20.6±2.9	26.3±2.8	S (10.7) 1.9 ^{''}
H4		12.1	3.0±0.5			15.8±2.5		F (20.8) 12.0 ^{''}
H5	P6	6.0	21.6±1.3	81.4±3.4	81.0±4.0	112.3±6.6	151.7±6.3	(G) IC 4329
H6	P7	13.6	0.9±0.3	4.5±0.9		4.9±1.5	8.4±1.7	S (19.9) 3.4 ^{''}
H11	P8	3.3	700.3±6.8	2746.4±44.2	2650.0±20.0	3645.0±35.6	5118.3±82.4	(G) IC 4329A
H15	P11	4.9	2.8±0.6	5.3±1.0		14.6±3.0	9.9±1.9	S (18.9) 2.0 ^{''}
H16	P12	1.0	3.5±0.5	12.7±1.4		18.2±2.7	23.7±2.6	S (17.6) 1.9 ^{''}
H17	P14	7.1	3.3±0.7	8.2±1.2		17.2±3.5	15.3±2.2	S (14.7) 2.2 ^{''}

scribed above were repeated for both the HRI and PSPC data, the observations being binned into 40 observation blocks.

Figs. 4 and 5 shows the results of this analysis for all the sources (except for the bright IC 4329A source) detected with both the HRI and the PSPC (Fig. 4 shows the results for the HRI, Fig. 5 for the PSPC). The layout of the figures is such that the coincident sources appear at the same position (hence H2 and H4 being coincident with P4). The results of the timing analysis for IC 4329A are shown in Fig. 6 (both HRI and PSPC).

Note that we are here interested in *variations* in the count rate from these sources, and not in the absolute values of these count rates, as these have been calculated earlier (Table 3). Hence we have been able to use small cut radii to avoid contamination from

neighbouring sources and concentrate at the very centres of each source. Differences in the calculated count rates between these two methods appear to be negligible, except in the HRI cases involving the very bright, extended sources, where reductions in count rate, from those given in Table 3, can be seen. This is to be expected, given the methods involved.

It appears that little in the way of any temporal variability exists for any of the bright sources (including that associated with IC 4329A), and this is borne out by fitting the light curves to constant flux values. Lightcurve H2, in fact, shows the largest deviation from consistency, a constant flux level fitting the data with a reduced χ^2 of 2.6. The H2 lightcurve therefore is variable only at the 2.1σ significance level (or at likelihood of 3.42). Thus

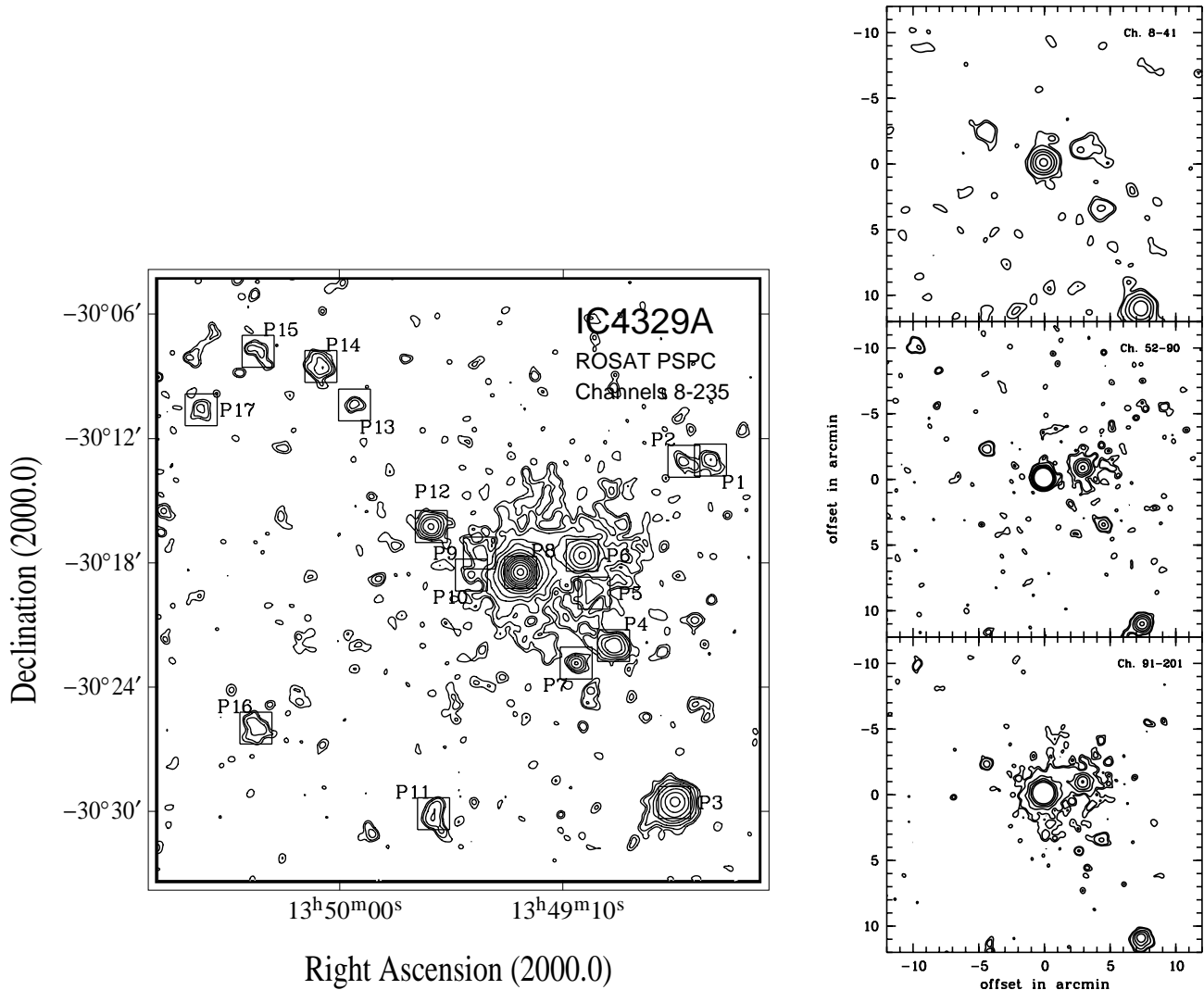


Fig. 3. ROSAT PSPC maps of the IC 4329A field in the broad (channels 8–235, corresponding approximately to 0.08–2.35 keV) band (main picture) and in the soft (channels 8–41), hard 1 (channels 52–90) and hard 2 (channels 91–201) bands (three smaller pictures). The contour levels in each figure are at 2, 3, 5, 9, 15, 31, 63, 127, 255, 511, 1023, 2047 and 4095σ (σ being 1.25×10^{-3} (broad), 1.49×10^{-3} (soft), 7.29×10^{-4} (hard 1) and 1.42×10^{-3} (hard 2) $\text{cts s}^{-1} \text{arcmin}^{-2}$) above the background (2.81×10^{-3} (broad), 3.40×10^{-4} (soft), 5.41×10^{-4} (hard 1) and 8.04×10^{-4} (hard 2) $\text{cts s}^{-1} \text{arcmin}^{-2}$). Source positions, as given in Table 2, are marked on the broad band image.

no significant variability is observed within any of the detected sources.

3. Results and discussion - the point sources

3.1. The bright point sources - IC 4329A, IC 4329 & H1-P3

The three bright sources visible in the IC 4329A field are all especially interesting. H1-P3 is bright, shows marginal evidence for extension in the PSPC (though the fact that no evidence for extension is seen in the HRI data implies that the source is truly unresolved) and appears associated with a quite bright (B magnitude = 16.5) star-like object, some $2.9''$ distant. H5-P6 is also very bright, appears to be significantly extended (both in the PSPC and HRI data), and is associated with the giant elliptical galaxy IC 4329. Finally, H11-P8 is extremely bright, showing

a great deal of structure, and is undoubtedly due to the Seyfert galaxy, IC 4329A.

It is worth noting again here that an analysis of the PSPC data (in conjunction with *COMPTON GRO* observations) has already been published by Madejski et al. (1995) (M95). They deal however, almost exclusively with the spectral properties of IC4329A (plus those of IC 4329 and H1-P3, or as they call it, S3), and so, in the discussion that follows, many of the results we present have not been addressed by M95, and are new, though we do compare the results of our spectral analysis with those of M95.

As in M95, spectra of all three bright objects (IC 4329A, IC 4329 and H1-P3) were analysed. Spectra were extracted for all three objects from within circles of $1.7'$ (for IC 4329A and IC 4329) and $3'$ (for H1-P3) at the position of each source (we note that an extraction radius of $3'$ for IC 4329A, as used in

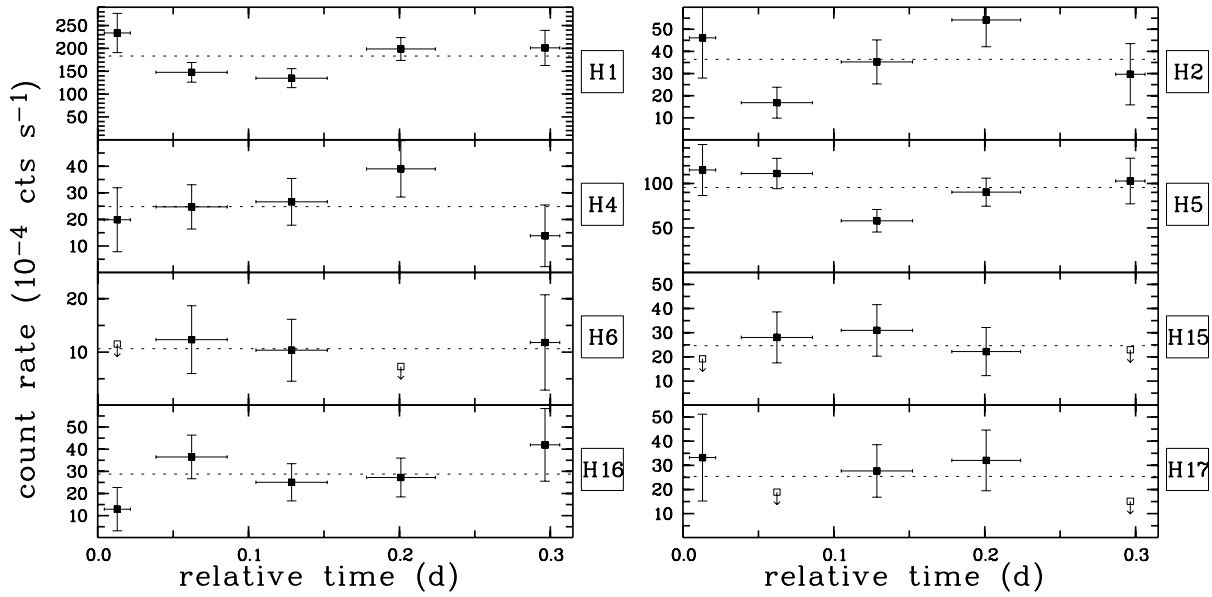


Fig. 4. ROSAT HRI lightcurves of the eight bright point sources detected with both the HRI and the PSPC (excluding IC 4329A) from Table 3. Observation times are 1.5, 4.1, 4.1, 3.9, and 1.7 ks. Count rates are shown by filled squares with 1σ error bars, and 2σ upper limits are shown by open squares. Dashed lines indicate the average count rate calculated over the complete observation.

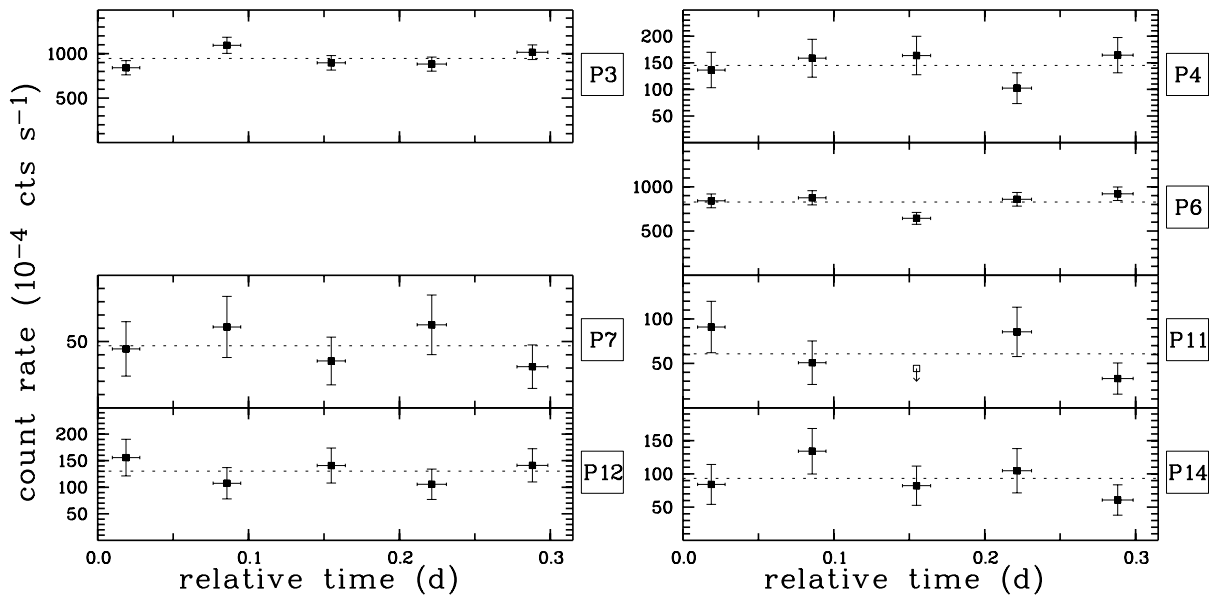


Fig. 5. ROSAT PSPC lightcurves of the seven bright point sources detected with both the HRI and the PSPC (excluding IC 4329A) from Table 3. Observation times are 1.6, 1.6, 1.6, 1.7, and 1.8 ks. Count rates are shown by filled squares with 1σ error bars, and 2σ upper limits are shown by open squares. Dashed lines indicate the average count rate calculated over the complete observation.

M95, is likely to be too large, given that this is approximately the distance between IC 4329A and IC 4329). Background spectra were extracted as follows: for IC 4329A, from an annulus $6.6'$ to $9.1'$ from IC 4329A, thus avoiding contamination from any other bright features; for IC 4329, from a $1.7'$ radius circle situated equidistant, on the opposite side of IC 4329A, thus ensuring that contamination from the very bright central source could be removed; and for H1-P3, from a $3'$ to $5.5'$ annulus centred on H1-P3, again avoiding any bright features.

The three background-subtracted spectra, once corrected for exposure and vignetting effects, were fitted with standard spectral models (thermal bremsstrahlung, power law, blackbody and Raymond & Smith (1977) hot plasma models). A number of extra, more complex models have been attempted as regards the IC 4329A spectrum, as in M95, and the results of all the best fits are given below in Table 4 as follows: Source (column 1), spectral model (whether PL - power law plus absorption, BB - blackbody plus absorption, PL/E - power law plus absorption

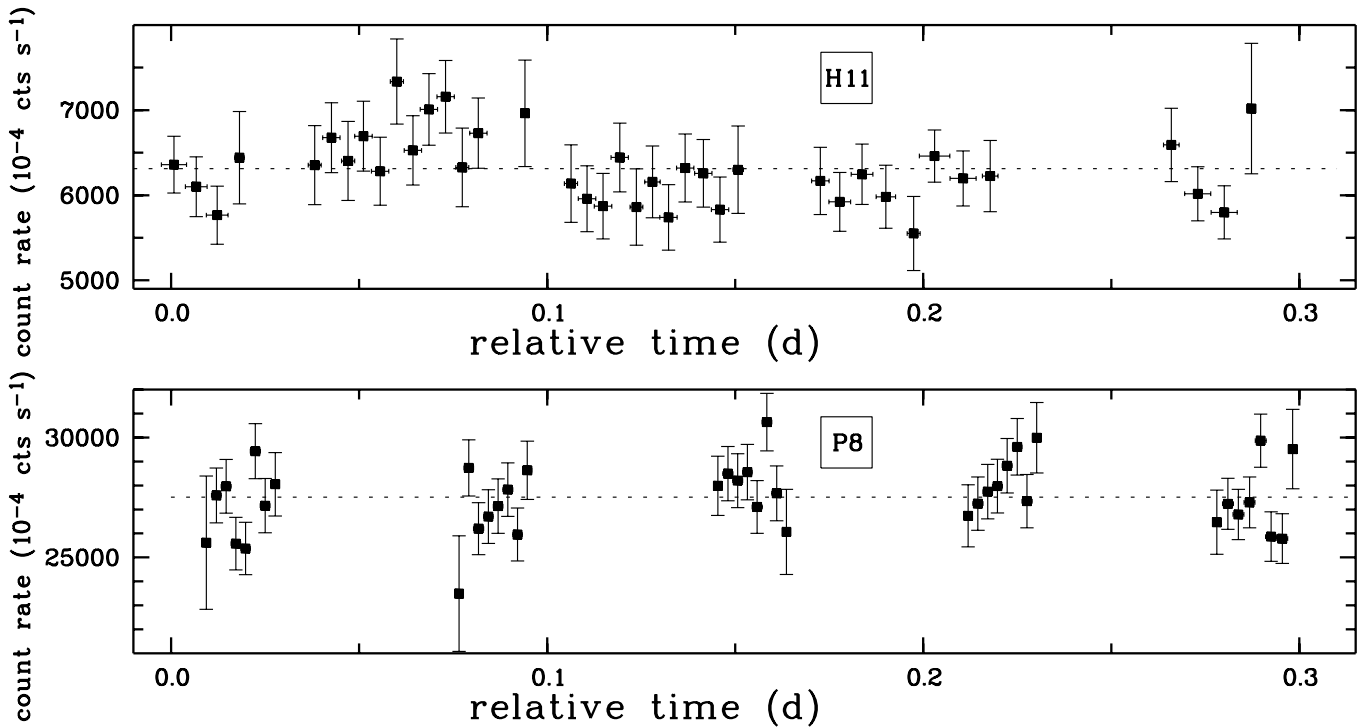


Fig. 6. ROSAT HRI (top) and PSPC (bottom) lightcurves of IC 4329A. The Observations were split into ≈ 400 s (HRI) and ≈ 200 s (PSPC) bins. Count rates are shown by filled squares with 1σ error bars, and the dashed lines indicate the average count rate calculated over the complete observation.

and an edge, RS Raymond & Smith hot plasma plus absorption) (column 2), fitted N_{H} (column 3), fitted spectral index Γ , where $F \propto E^{-\Gamma}$ (column 4), fitted temperature (kT, in keV) (column 5) (Note here that in the case of the PL/E model, this column gives the edge energy in keV). The next columns give the metallicity (solar, where an ‘F’ indicates that the value has been frozen) (column 6), the reduced χ^2 (column 7), and three values of the (0.1–2.4 keV) luminosity (columns 8–10). Two values of luminosity as calculated using the PSPC results are given; one (column 8) gives the ‘intrinsic’ luminosity of the source (i.e. correcting for the total N_{H}), the second (column 9) gives an ‘emitted’ luminosity (i.e. correcting merely for the Galactic N_{H}). The final luminosity column (column 10) gives the intrinsic (0.1–2.4 keV) luminosity, using the count rate observed with the HRI, and calculating the fluxes, assuming identical spectral models as inferred from the PSPC data. All luminosities are calculated for an assumed distance of 64 Mpc (which is almost certainly incorrect in the case of H1-P3, as discussed below).

Although no thermal model (whether a Raymond & Smith hot plasma model or a thermal bremsstrahlung model) is able to fit the IC 4329A data adequately, a simple power law model does give quite an acceptable fit, the fitted parameters agreeing well with M95 and with Rush et al. (1996). However, as in M95, close inspection of the residuals does suggest an edge-like feature at around 0.7 keV. Incorporating this edge into the model does improve the fit (the data and residuals are shown in Fig. 7), and we are able to reproduce the best-fit results of M95 very accurately. Firstly, a photon index of 1.73 ± 0.33 is

suggested, consistent with M95, with the *Ginga* data (Piro et al. 1990; Fiore et al. 1992), and with the *ASCA* data (Cappi et al. 1996). Secondly, the edge feature at 0.72 ± 0.07 keV is found at exactly the same energy as in M95. As M95 suggest, the energy of this edge is inconsistent with that expected if there were a neutral absorber present, and this strongly suggests the presence of an ionized absorber (OVI, OVII). Further modelling, to address the question of the true nature of this absorber, is possible. However, because of the modest spectral resolution of the PSPC, one cannot distinguish between different models, i.e. between an ionized absorber model, a partial covering by neutral material model, and a high column cold absorber model (see M95 for a detailed discussion).

It is worth noting that the inferred N_{H} , $27.9 \times 10^{20} \text{ cm}^{-2}$, is substantially larger than the Galactic N_{H} in the direction of IC 4329A ($4.4 \times 10^{20} \text{ cm}^{-2}$; Dickey & Lockman 1990), indicating the presence of a large intrinsic absorption. This is not too surprising given the edge-on nature of the galaxy. In their study of the soft X-ray properties of Seyfert galaxies in the ROSAT All-Sky Survey, Rush et al. (1996) also find a very significant excess in the best fit N_{H} .

The intrinsic (0.1–2.4 keV) luminosity of IC 4329A, $6.3 \times 10^{43} \text{ erg s}^{-1}$, is very large, within the top 10% or so of the Seyferts within the Rush et al. (1996) All-Sky Survey sample. It is an extremely luminous galaxy, and an extremely luminous Seyfert galaxy as well.

The IC 4329 spectrum on the other hand, is only fitted adequately well by a thermal (Raymond & Smith hot plasma)

Table 4. Results of the best model fits to the IC 4329A, IC 4329 and H1-P3 spectra (see text). Models are: PL (power law plus absorption), BB (blackbody plus absorption), PL/E (power law plus absorption and an edge), RS (Raymond & Smith hot plasma plus absorption). In the case of the PL/E fit, the temperature kT refers to the temperature of the edge. Three (0.1–2.4 keV) luminosities are tabulated. One, the intrinsic PSPC luminosity of the source, two, the Galactic N_{H} -corrected (i.e. emitted) PSPC luminosity (Galactic $N_{\text{H}} = 4.4 \times 10^{20} \text{ cm}^{-2}$), and lastly, the intrinsic HRI luminosity, using the HRI count rates in conjunction with the models suggested by the PSPC data.

Source	Model	N_{H} 10^{20} cm^{-2}	Photon Index	kT (keV)	Z (Solar)	red. χ^2	L_{x} ($10^{42} \text{ erg s}^{-1}$)		
							(Intrinsic)	(Emitted)	HRI (Intrinsic)
(1)	(2)	(3)	(4)	(5)	(6)	(7)	(8)	(9)	(10)
IC 4329A	PL	22.7 ± 3.3	1.28 ± 0.12			1.1	41.6 ± 0.7	23.7 ± 0.4	29.0 ± 0.3
	BB	7.5 ± 0.1		0.52 ± 0.02		1.1	23.8 ± 0.4	22.8 ± 0.4	16.6 ± 0.2
	PL/E	27.9 ± 5.1	1.73 ± 0.33	(0.72 ± 0.14)		0.9	63.0 ± 1.0	23.4 ± 0.4	43.0 ± 0.5
IC 4329	RS	2.7 ± 1.2		1.08 ± 0.06	1.0(F)	1.3	0.64 ± 0.02	0.64 ± 0.02	0.53 ± 0.03
	RS	4.3 ± 1.6		1.07 ± 1.07	0.4 ± 0.2	1.3	0.79 ± 0.03	0.79 ± 0.03	0.61 ± 0.04
H1-P3	PL	3.2 ± 1.3	2.35 ± 0.33			1.4	1.04 ± 0.04	1.04 ± 0.04	0.67 ± 0.05

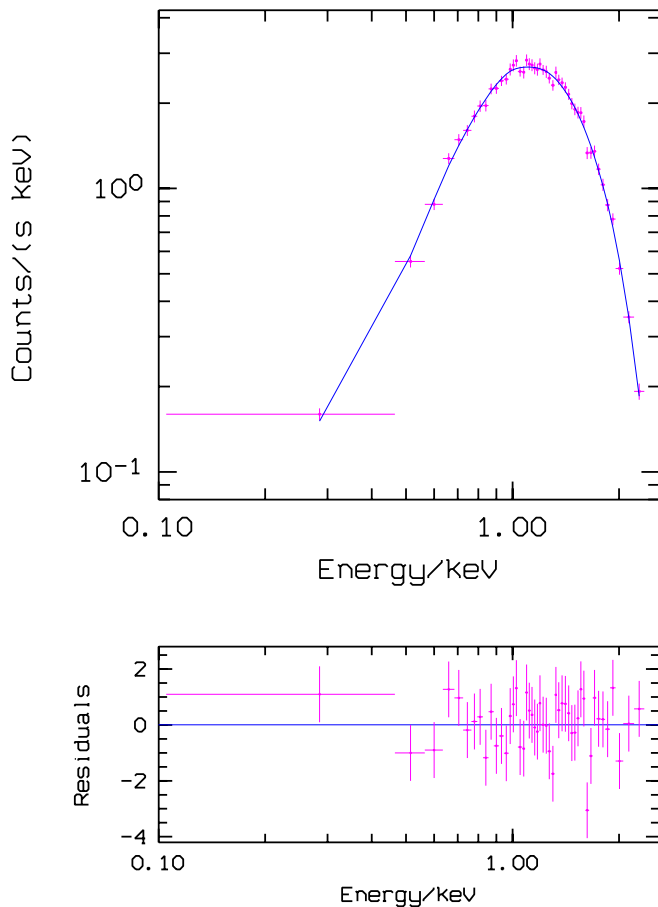


Fig. 7. IC 4329A spectrum with the best-fit power-law plus absorption edge model (see Table 4). The pulse height spectrum of the total X-ray emission is indicated by crosses, and the fit, by the solid line.

spectrum. The best fit, while keeping the metallicity frozen at solar, results in a well-constrained, 1.08 ± 0.06 keV spectrum, absorbed by a column of $2.7 (\pm 1.2) \times 10^{20} \text{ cm}^{-2}$, a column consistent with (though on the low side of) the Galactic value. This result is entirely consistent with M95. Fitting of the spectrum while letting the metallicity optimize, gives a column entirely

consistent with the Galactic value and a low (0.4 ± 0.2 solar) metallicity, though the fitted temperature is less well constrained than in the frozen-metallicity case. The intrinsic (0.1–2.4 keV) luminosity of IC 4329, $7.9 \times 10^{41} \text{ erg s}^{-1}$, is somewhat higher than average when compared to optically similar systems (Fabiano et al. 1992). The fitted temperature is entirely consistent with that of ellipticals, *ASCA* observations resulting in temperatures for several early-type galaxies of between 0.7 and 1.2 keV (Matsushita et al. 1994; Rangarajan et al. 1995). Similarly, the low fitted metallicity appears to be consistent with ellipticals, high-resolution studies with *ASCA* revealing abundances ≤ 0.5 solar in several cases (Loewenstein et al. 1994; Matsushita et al. 1994).

The H1-P3 spectrum is best fit with a power law model of photon index 2.35 ± 0.33 , absorbed by a column of $3.2 (\pm 1.3) \times 10^{20} \text{ cm}^{-2}$, consistent with that out of our own Galaxy. It is almost certainly due to a background quasar, given the facts that it is unresolved in the HRI data, it appears coincident with a quite bright (B mag = 16.5) star-like object, and it has a spectrum consistent with that of quasars (power law with photon indices in the range 2.2 ± 0.2 ; Branduardi-Raymont et al. 1994; Roche et al. 1995).

Finally, note that, in Table 3, it appeared that, in the cases of these bright sources, the inferred HRI and PSPC fluxes did not agree particularly well. This could have been attributable to time-variability or the assumption of the wrong spectral model. We have already seen however (Figs. 4–6) that none of these sources appear to be particularly time-variable in either the HRI or the PSPC, and usage of the correct spectral model, as has been done here, has only really aided the situation in the case of IC 4329, and then, only slightly. In the case of H1-P3, it is possible that the source has varied between the HRI and PSPC observations. The fact that the object is very likely to be a QSO or background AGN adds some credence to this. Also bare in mind that the quality of fit to the H1-P3 PSPC spectra is not excellent, the reduced χ^2 being only 1.4. In the case of IC 4329A and IC 4329, the situation is rather intriguing. Both sources appear extended however, and this will lead to a reduction in the calculated HRI count rates, compared to the PSPC count

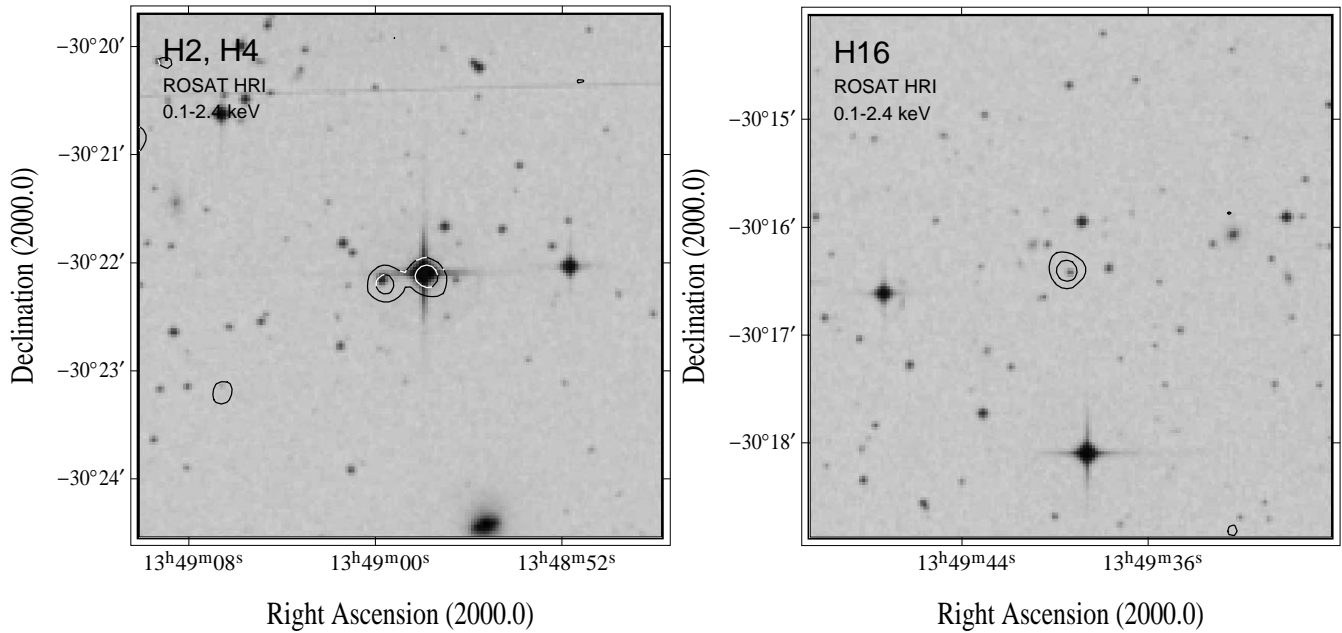


Fig. 8. Contours of HRI emission overlaid onto optical digitized sky survey images for the H2/H4 field (left) and the H16 field (right). The X-ray image has been smoothed with a Gaussian filter of $10''$ FWHM, and the contours correspond to 0.0625 and 0.1875 cts arcsec $^{-2}$.

rates. Furthermore, IC 4329A is extremely bright, accentuating the above effect. Finally, as may be the case (Fig. 2), and is discussed in detail later, if there were a large amount of low-surface brightness, diffuse emission in the vicinity of these two galaxies, this could very well lead to a reduction in the HRI count rates compared to the PSPC count rates, the HRI being relatively far less sensitive to this type of emission than the PSPC.

3.2. The secondary point sources

Moving on to the remaining point sources, many interesting results have been obtained. Feature P4, for instance, appears elongated in the east-west direction in the PSPC image (Fig. 3). The HRI is able to resolve this feature into two separate, equally bright sources (H2 and H4), the more western of which (H2) appears coincident with a bright stellar-like object, with a B magnitude of 10.7. The apparent optical counterpart to H4 (not seen in the APM finding charts of Irwin et al. (1994)) is much fainter ($B=14.7$, see Fig. 8(left)). What is rather striking though, is that, what appears to be a ‘twin’ of H2/H4-P4 can be seen on the opposite side of IC 4329A, at an extremely similar projected distance from the bright central galaxy. This source, H16-P12, appears coincident with a rather faint ($B=17.6$) stellar-like object, less than $2''$ west of HRI position (Fig. 8(right)). The positioning of these two sources with respect to the central bright galaxy, IC 4329A, is both unusual and intriguing.

On July 6, 1997, during an observing campaign at the 2.2m ESO/MPG telescope at La Silla observatory, we obtained spectra of these optical candidates using the EFOSC2 spectrograph with grism #4, a $2''$ -wide long slit and the 2048×2048 $15\mu\text{m}$ LORAL CCD. This gave a dispersion of 2 \AA per pixel, a spec-

tral coverage of $4100\text{--}7500 \text{ \AA}$, and a spectral resolution of 12 \AA FWHM. The seeing was typically $1.5''$. The data were reduced according to the procedure given in Pietsch et al. (1998).

Through these optical observations, we have established that all three sources have nothing at all to do with IC 4329A, and are in fact Galactic foreground or background objects. Sources H2 and H4 to the south-west, when compared with Jacoby et al.’s (1984) library of stellar spectra, appear to be foreground stars of types G3 V and M5 V respectively. Furthermore, the north-eastern source looks to be a background quasar with a redshift of 0.5430 ± 0.0005 . The HRI count rates measured are consistent with the X-ray fluxes expected from these source classes.

All of the remaining non-bright sources appear to have very close ($< 3.5''$) optical counterparts, the brightest of which is that associated with H17-P14 ($B=14.7$).

4. Results and discussion - the unresolved emission

What is very evident from Fig. 3 is that there appears to be a great deal of unresolved emission enveloping the sources associated with the two central galaxies, IC 4329A (P10) and IC 4329 (P8). As seen earlier, this is not seen at first with the HRI (Fig. 1), though becomes strikingly clear when an adaptive filtering technique is applied (Fig. 2). The fact that this emission is very obvious in the unfiltered PSPC data, though this fact is not mentioned in M95, is very encouraging, and to investigate this aspect of the X-ray emission further, a similar filtering technique was applied to the PSPC data. An image (of pixel size $15''$, and over the broad 11-235 range) was formed, and sections of the image were smoothed using progressively larger Gaussians for lower intensity pixels. Pixels of amplitude 1 (2,3,4,5,6,7,8) were smoothed with a Gaussian of FWHM

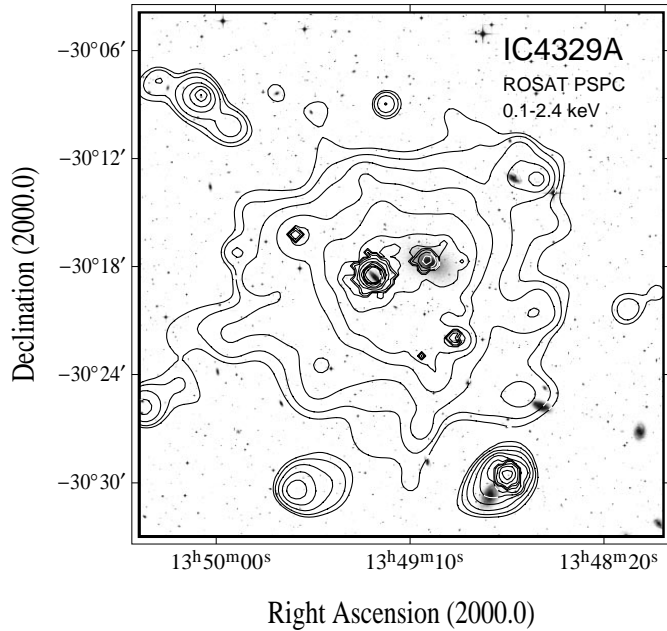


Fig. 9. ROSAT (0.1–2.4 keV) PSPC map of the IC 4329A field obtained using an adaptive filtering technique (see text), overlaid on a digitized sky survey image. The contour levels are at 2, 3, 5, 9, 15, 31, 63, 127, 255, 511, 1023 and 2047σ (σ being 8.3×10^{-5} cts s^{-1} arcmin $^{-2}$) above the background (1.3×10^{-3} cts s^{-1} arcmin $^{-2}$).

320'' (225,160,115,80,55,40,30)''). Again, pixels of amplitude greater than 8 remained unsmoothed, to ensure that the bright point sources were not smoothed into the background. The resultant image is shown in Fig. 9. Again, as in the adaptively smoothed HRI image, a great deal of unresolved emission is apparent, extending to a much greater radius than is seen in the equivalent HRI image (9' compared to 5'). This is not too surprising, even taking into account the factor of ~ 2 deficit in exposure times, as the PSPC is far more sensitive to low surface brightness diffuse emission than the HRI.

As the PSPC has some spectral resolution, we are able to investigate the spectral properties of this unresolved emission. What was immediately apparent though, before any rigorous spectral fitting (as described later) was performed, was that this unresolved emission appeared markedly two-component. It was decided at first to investigate the spatial properties of these two components, to try and ascertain their distributions.

4.1. The unresolved emission - spatial properties

This two component nature is apparent in Fig. 10. Shown are two images, each essentially the same as Fig. 9, but extracted from two separate energy bands, the first (soft), extracted from channels 8–41, the second (hard) extracted from channels 52–201. In both cases, images with 15'' resolution were formed and these images were smoothed using progressively larger Gaussians for lower intensity regions. Pixels of amplitude 1 (2,3,4,5,6,7,8) were smoothed with a Gaussian of FWHM 320'' (225,160,115,80,55,40,30)'' , and pixels of amplitude greater

than 8 were not smoothed, ensuring that the bright point sources were not smoothed into the background).

The results of this procedure are really rather striking, and the two components, the soft and the hard components, show remarkably different properties. The soft component is dominated by IC 4329A and the bright H1-P3 source to the south-west. Strong features are also seen associated with IC 4329, with the two outlying sources, H2/4-P4 and H16-P12, and with H15-P11. The *unresolved* soft emission though, which is what we are here most interested in, appears almost entirely to the south-east of the bright IC 4329A source, in a roughly semi-circular distribution, 'centred' on IC 4329A, and extending out past the two outlying sources H2/4-P4 and H16-P12. The emission appears far from uniform, containing much structure, notably in the south-east direction, perpendicular to the IC 4329A disc (and to the line joining the two outlying sources to IC 4329A). Some evidence exists for a similar (though very much smaller) extension to the north-west of IC 4329A, though much of this emission may be due to IC 4329.

As regards the hard emission, many sources, notably IC 4329A, IC4329, H1-P3, and the two outlying sources, appear as strong sources. The unresolved hard emission however, appears markedly different to the unresolved soft X-ray structure. Firstly, it extends not only to the south-east, as the soft component does, but also to the north-west, and appears roughly circular in nature. Furthermore, in contrast to the soft component, it appears rather uniform and smooth, with little in the way of substructure. Interestingly, and as discussed later, the hard component is not centred on IC 4329A, but instead appears to be centred somewhere between the IC 4329A/IC 4329 pair. Also of note is the fact that this emission is seen to envelope two further galaxies within the galaxy group mentioned in the introduction. These two galaxies, IC 4327 to the north-west of the IC 4329A/IC 4329 pair, and NGC 5298 to the south-west, can be seen at the edge of the hard unresolved emission (Fig. 10).

Structure in the unresolved emission is evident also in the HRI data. Fig. 11 shows contours of HRI X-ray emission superimposed on an optical image of the two central galaxies. A 3'' resolution image was extracted from the HRI channel range 6–11, and smoothed with a Gaussian of FWHM 7''. Firstly, as regards the above discussion, significant emission, in what appears to be in the form of a 'bridge' (with a curious northern plume), is seen connecting the two galaxies. Secondly, with regard to the emission surrounding IC 4329A, there appears to be an elongation along the disc, pointing towards the two outlying sources, one of which, H2/4-P4, can be seen at the bottom-right of Fig. 11. Also, there appears to be good evidence for an extension perpendicular to the IC 4329A disc, especially, as seen in the PSPC soft band image above, to the south-east. Lastly, as regards IC 4329, the curious spiral-arm-like structure to the X-ray emission is very intriguing.

4.2. The unresolved emission - spectral properties

It appears therefore, that the unresolved emission within the IC 4329A/IC 4329 system is two-component, and this two com-

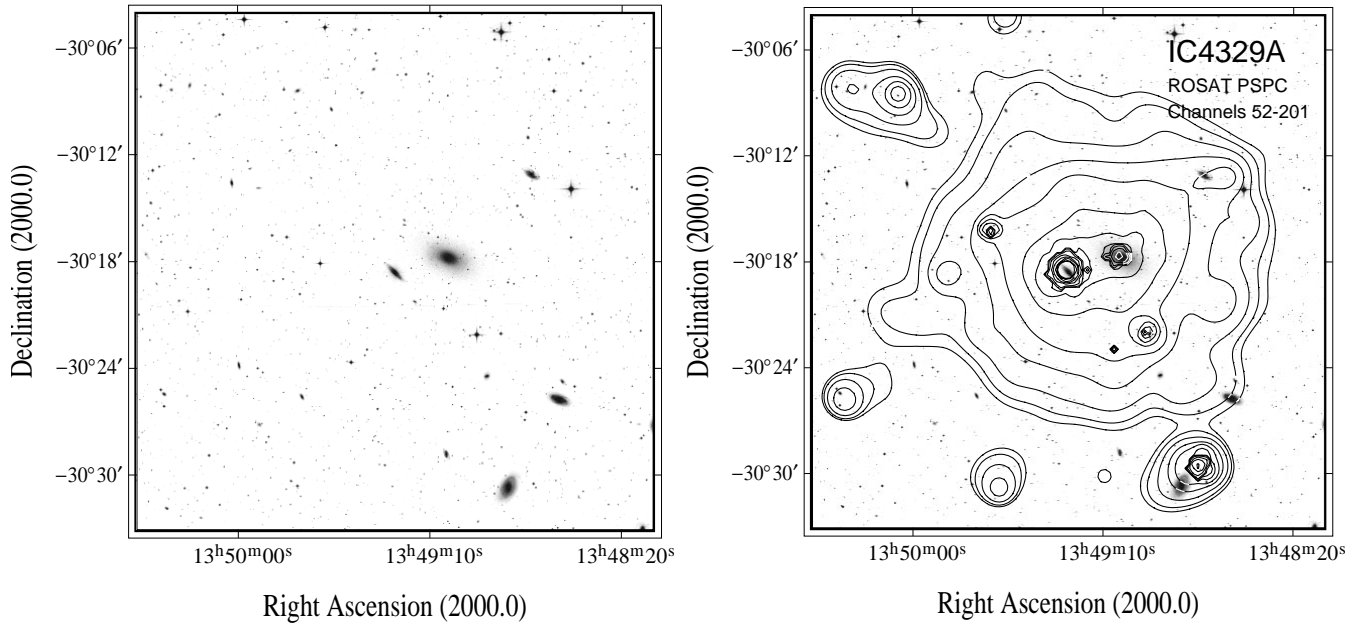


Fig. 10. ROSAT PSPC maps of the IC 4329A field in the (left) soft (channels 8–41) and (right) hard (channels 52–201) bands, obtained using an adaptive filtering technique (see text), and overlaid on optical images. The contour levels are at 2, 3, 5, 9, 15, 31, 63, 127, 255, 511, 1023 and 2047σ (σ being 2.3×10^{-5} (soft) and 4.3×10^{-5} (hard) $\text{cts s}^{-1} \text{arcmin}^{-2}$) above the background (7.1×10^{-4} (soft) and 6.4×10^{-4} (hard) $\text{cts s}^{-1} \text{arcmin}^{-2}$).

ponent nature varies across the system, the area to the north-west of the IC 4329A disc being hard, the area to the south-east, being hard also, but with a very significant soft component contribution. This north-west/south-east divide was used to investigate the spectral properties of the unresolved emission. Several unresolved emission spectra were extracted, both from the north-west (NW) and the south-east (SE) side, a line through the centre of IC 4329A, at an angle (anticlockwise from north) of 56° (so that it approximately followed both the IC 4329A disc and the line joining the two outlying sources to IC 4329A), used to separate the two halves. Two main spectra (NW and SE) were extracted from half-annuli centred on IC 4329A, with inner radii of $2.25'$ and outer radii of $11.7'$, and were binned to give a signal-to-noise ratio of approximately six in each channel. These two spectra were each further subdivided into three concentrically-extracted spectra, with inner and outer radii of $2.25' - 5'$ (NW1 and SW1), $5' - 8.25'$ (NW2 and SW2) and $8.25' - 11.7'$ (NW3 and SW3). These six sub-spectra were each binned to give a signal-to-noise ratio of approximately five in each channel. In the extraction of each of these 8 total spectra, data associated with each of the sources were excluded to a radius of $1.5'$. A background spectrum, free of unresolved emission, was extracted from a $15' - 18.25'$ annulus, data associated with the sources excluded to a radius of $2'$. Once these spectra were corrected for background and exposure time, it was possible to gauge the soft and hard-band contributions within each area. In the north-west, the percentage of counts in the soft ($0.1 - 0.5$ keV) band, compared to the total ($0.1 - 2.4$ keV) number of counts, is seen to be low ($\approx 8.5\%$) and constant (to within $\sim 3\%$) for each of the three spectra (NW1, NW2, NW3). In the south-east however, the soft band contribution is seen to

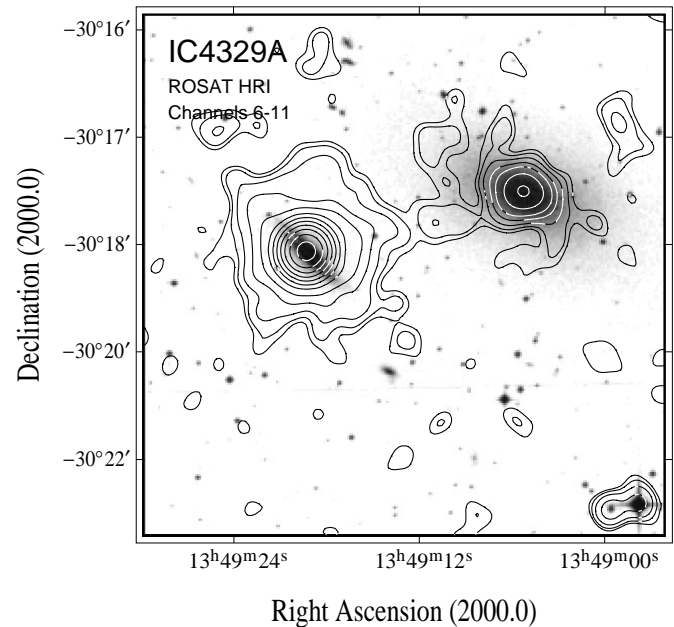


Fig. 11. ROSAT HRI map of the IC 4329A field obtained using an adaptive filtering technique (see text), overlaid on a digitized sky survey image. Only channels 6–11 are used. The contour levels are at 2, 3, 5, 9, 15, 31, 63, 127, 255, 511, 1023 and 2047σ (σ being $7.1 \times 10^{-4} \text{cts s}^{-1} \text{arcmin}^{-2}$) above the background ($2.1 \times 10^{-3} \text{cts s}^{-1} \text{arcmin}^{-2}$).

rise sharply from 19.7% for the inner-extracted spectrum (SE1), through 34.8% for SE2, to 53.6% for SE3.

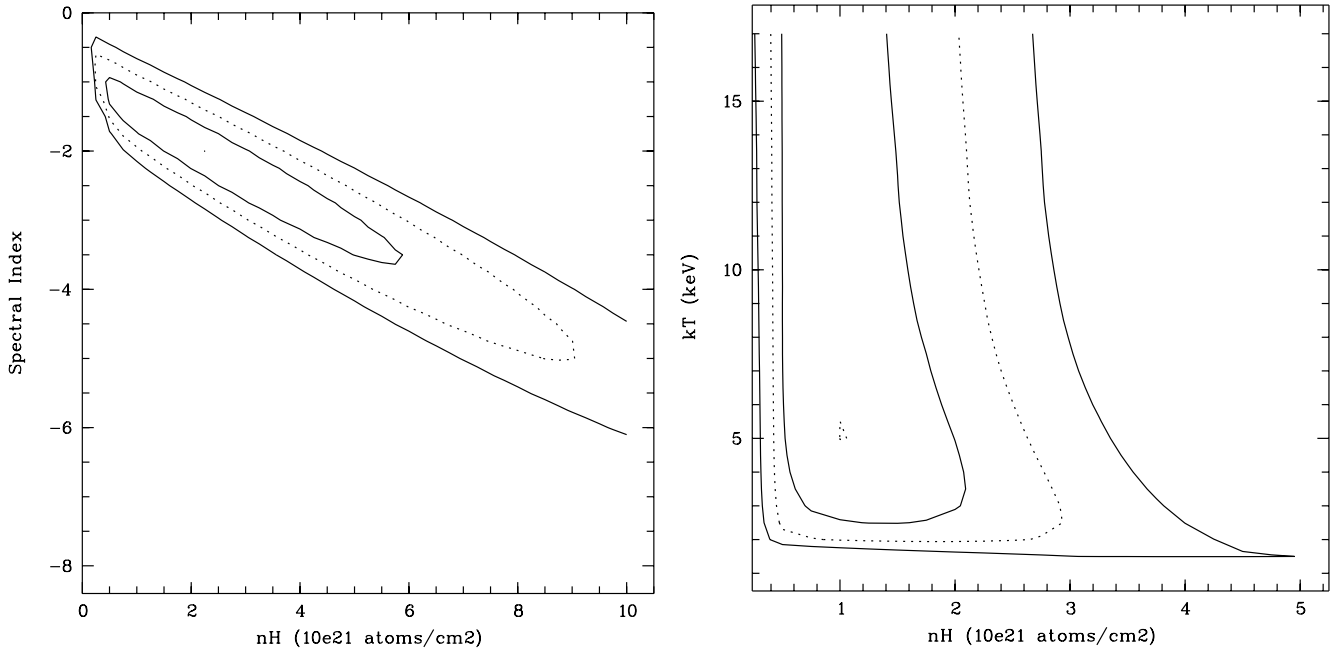


Fig. 12. Model spectrum fits to the NW spectrum. (Left) Gaussian contour levels of 1σ , 2σ and 3σ in the spectral index – absorption column plane for the power-law fit to the NW spectrum (Table 5, column 1). (Right) Gaussian contour levels of 1σ , 2σ and 3σ in the temperature – absorption column plane for the Raymond & Smith plasma fit to the NW spectrum (Table 5, column 1).

As in the fitting of the point source spectra, spectral models were fitted to these unresolved emission spectra. Dealing first with the north-west spectra, power-law, and Raymond & Smith hot plasma models were first attempted, and the results of the best fits are summarized in Table 5. As can be seen, power-law models (columns 2-6) are able to fit not only the NW spectrum, but also the three separate NW1, NW2 and NW3 spectra, very well, with reduced χ^2 s of less than unity (in fact more like 0.5 in every case, apart from NW2). Though the resulting parameters at first appear rather different, the errors are rather large, and the spectral fit parameters are quite consistent with one another, i.e. the north-western spectrum appears to remain constant with radius. Fig. 12 (left) shows the 99%, 95% and 68% confidence contours in the absorbing column – spectral index plane for the power-law fit to the full NW spectrum (i.e. Table 5, row 1).

One should note here the bottom four power law fits, given in Table 5, the implications of which are discussed more fully later. Here, an attempt has been made to see how consistent the NW spectra are with the spectrum of the bright central source IC 4329A. Upon freezing the absorption column at the value obtained in the fitting of the IC 4329A spectrum ($22.7 \times 10^{20} \text{ cm}^{-2}$, see Table 4), the quality of each fit is seen to remain very good. The values obtained for the spectral index however, though consistent with each other, are somewhat higher than the IC 4329A value.

Moving on now to the Raymond & Smith hot plasma model fits to the NW spectra (columns 7-11), the quality of the fits is again good, in the majority of cases. The absorbing column appears to be small and is consistent with the Galactic value in every case. Unfortunately, as regards the temperature,

little definite information can be gleaned from these results, whether the absorbing column is left to optimize or is frozen at the Galactic value. Though the fitted temperatures appear to be high, the fitting procedure often ‘pegging’ the temperature at the highest allowable value, the errors are large. The size of this error region can be seen in Fig. 12 (right), where 99%, 95% and 68% confidence contours are shown in the absorbing column – temperature plane for the Raymond & Smith hot plasma model fit to the full NW spectrum (i.e. Table 5, row 1).

Finally, it is worth noting that usage of a thermal bremsstrahlung model in the spectral fitting gives very similar results to the Raymond & Smith results. The equivalent absorbing column – temperature confidence grid appears essentially identical to Fig. 12 (right). Only in the fitting to the total NW spectrum was a best fit realised – $N_{\text{H}} = 16.5^{+23.0}_{-11.4} \times 10^{20} \text{ cm}^{-2}$, $kT > 1.05 \text{ KeV}$, with a reduced χ^2 slightly worse than for the Raymond & Smith case (0.54, with 9 degrees of freedom).

The emission to the south-west, as mentioned previously, is considerably more complicated, requiring a two-component model to fit the spectra, even adequately (the best one-component power-law and Raymond & Smith hot plasma fits to the SE spectrum result in reduced χ^2 s of over 5 and 7, respectively). Freezing of a number of the components was necessary, as too many free parameters led to fits that either refused to settle at consistent values or had huge error regions. Following the line of thought touched upon above, the hard component was assumed to be identical to the IC4329A spectrum. The variation of the spectral parameters can be seen in Fig. 13. Here, the 99%, 95% and 68% confidence contours in the soft-component absorption column – temperature plane are shown for the full SE

Table 5. Results of fitting power-law and Raymond & Smith hot plasma models to the north-western unresolved emission spectra (see text), as follows: Column 1 gives the spectrum, whether the full NW spectrum or one of NW1, NW2, or NW3, the radially extracted spectra. Columns 2–6 give the results of the best power-law fits; fitted N_{H} (column 2), fitted spectral index, Γ , where $F \propto E^{-\Gamma}$ (column 3), and the reduced χ^2 and number of degrees of freedom (column 4). Columns 7–9 give the results of the best Raymond & Smith hot plasma model fits (with the metallicity frozen at the solar value); fitted N_{H} (column 7), fitted temperature kT, in keV (column 8), and the reduced χ^2 and number of degrees of freedom (column 9). Where parameters are seen to ‘peg’ at the highest or lowest allowable values, 2σ upper or lower limits are given. Two values for the (0.1–2.4 keV) X-ray luminosity (scaled to account for the emission lost in the ‘holes’ left after the source subtraction procedure) are each given (corresponding to a distance of 64 Mpc) in columns 5 and 6 (for the power-law fits) and columns 10 and 11 (for the hot plasma fits). Cols. 5 and 10 give the ‘intrinsic’ luminosity (correcting both for Galactic and intrinsic absorption), while columns 6 and 11 give the ‘emitted’ luminosity (i.e. correcting merely for the Galactic N_{H}).

Spec.	Power-law model					Raymond & Smith model				
	N_{H} (10^{20} cm^{-2})	Photon Index	red. χ^2 (n.d.o.f.)	L_{x} ($10^{41} \text{ erg s}^{-1}$) (Int.)	L_{x} ($10^{41} \text{ erg s}^{-1}$) (Em.)	N_{H} (10^{20} cm^{-2})	kT (keV)	red. χ^2 (n.d.o.f.)	L_{x} ($10^{41} \text{ erg s}^{-1}$) (Int.)	L_{x} ($10^{41} \text{ erg s}^{-1}$) (Em.)
(1)	(2)	(3)	(4)	(5)	(6)	(7)	(8)	(9)	(10)	(11)
NW	$22.0^{+36.5}_{-17.5}$	$2.03^{+1.65}_{-1.15}$	0.55(9)	26.3	8.67	$10.0^{+13.5}_{-5.00}$	> 1.9	0.50(9)	8.80	6.08
NW1	$3.60^{+27.5}_{-0.20}$	$0.96^{+1.60}_{-0.30}$	0.48(5)	4.69	4.69	$5.90^{+15.4}_{-3.30}$	> 1.9	0.69(5)	3.75	3.24
NW2	$48.3^{+77.0}_{-42.5}$	$3.15^{+2.33}_{-2.10}$	0.95(7)	72.8	2.90	$16.4^{+32.2}_{-10.5}$	$2.62^{+11.1}_{-1.00}$	0.84(7)	3.50	2.07
NW3	< 110	$1.09^{+2.15}_{-1.09}$	0.41(3)	3.13	3.13	< 55	> 1.6	2.38(3)	2.77	2.77
NW	22.7(F)	2.06 ± 0.37	0.50(10)	27.4	8.63	4.40(F)	> 2.4	0.71(10)	7.91	7.91
NW1	22.7(F)	1.97 ± 0.50	0.75(6)	11.1	3.79	4.40(F)	> 2.2	0.61(6)	3.46	3.46
NW2	22.7(F)	1.99 ± 0.51	0.91(8)	9.66	3.26	4.40(F)	$2.59^{+7.2}_{-0.6}$	1.24(8)	2.66	2.66
NW3	22.7(F)	2.07 ± 0.89	0.62(4)	7.38	2.31	4.40(F)	> 2.0	0.34(4)	2.16	2.16

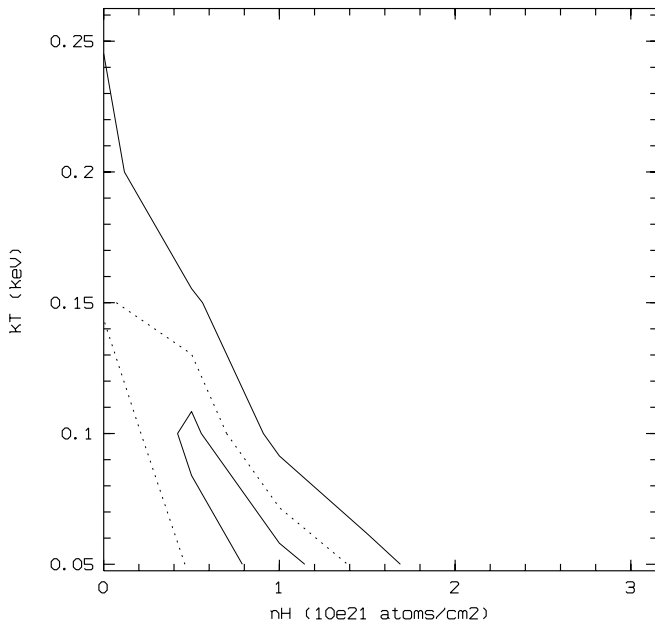


Fig. 13. Gaussian contour levels of 1σ , 2σ and 3σ in the soft-component temperature–absorption column plane for the (hard) power-law plus (soft) Raymond & Smith plasma fit to the SE spectrum.

spectrum, i.e. the hard component is frozen to that of IC4329A, and the metallicity of the soft component is frozen at the solar value.

As can be seen, the soft component appears to be very soft, and rather unabsorbed. Fitting of the three sub-spectra SE1, SE2 and SE3, failed to settle at consistent values, and it is only when the absorption column of the soft component is fixed at

the Galactic value ($4.40 \times 10^{20} \text{ cm}^{-2}$), as seems completely reasonable from Fig. 13, that good fits are obtained. Table 6 summarizes these best two-component (power-law plus Raymond & Smith hot plasma) model fits to the SE spectra. In actuality, whatever (within reason) the hard component is frozen at (for instance, the higher index fit to the NW spectra - see Table 5), or whether the soft-component metallicity is frozen or left free, makes very little difference to the resultant fits. Assuming therefore that a hard component somewhat similar (if not identical) to the IC4329A spectrum is present, then a soft component, consistent with a very cool, relatively (if not completely) unabsorbed hot plasma, appears to be present. It is also worth noting here, that the equivalent confidence contour plots for the three sub-spectra SE1, SE2 and SE3, appear more-or-less identical, though with larger-spaced contours reflecting the reduction in statistics.

Models incorporating two Raymond & Smith hot plasmas either failed to converge or, if they did, the results obtained were unphysical or had uncomfortably large error regions. It is worth noting that a model incorporating two thermal bremsstrahlung models, both with absorbing columns frozen at the Galactic value, is able to fit the SE spectrum. A very low and a very high temperature plasma is required.

As we have seen therefore, both a hard and a soft component to the unresolved emission appear to exist around IC 4329A, the hard component lying, rather smoothly and symmetrically distributed, around the IC 4329A/IC 4329 pair, the soft component lying almost entirely to the south-east of IC 4329A. As we have regions of emission where only the hard emission appears to exist (to the north-west), it is easier to deal with this aspect of the emission first. Only after this, can we move on to discuss the soft emission component.

Table 6. Results of fitting two-component (power-law + Raymond & Smith hot plasma) models to the south-eastern unresolved emission spectra (see text), as follows: Column 1 gives the spectrum, whether the full SE spectrum or one of SE1, SE2, or SE3, the radially extracted spectra. Columns 2 and 3 give the parameters of the power-law component to the best fit; fitted N_{H} (column 2), and fitted spectral index, Γ , where $F \propto E^{-\Gamma}$ (column 3). Columns 4 and 5 give the parameters of the Raymond & Smith hot plasma component of the best fit (with the metallicity frozen at the solar value); fitted N_{H} (column 4), and fitted temperature kT, in keV (column 5). The reduced χ^2 and number of degrees of freedom are given in (column 6). Two values for the (0.1–2.4 keV) X-ray luminosity (scaled to account for the emission lost in the ‘holes’ left after the source subtraction procedure) are given (corresponding to a distance of 64 Mpc) in columns 7 and 8. column 7 gives the ‘intrinsic’ luminosity (correcting both for Galactic and intrinsic absorption), and column 8 gives the ‘emitted’ luminosity (i.e. correcting merely for the Galactic N_{H}), the figures in brackets indicating the percentage contribution to this luminosity from the Raymond & Smith hot plasma (i.e. the soft) component.

Spectrum	Power-law component		Raymond & Smith component		red. χ^2 (n.d.o.f.)	L_{x} (10^{41} erg s $^{-1}$)	
	N_{H} (10^{20} cm $^{-2}$)	Photon Index	N_{H} (10^{20} cm $^{-2}$)	kT (keV)		(Int.)	(Em.)
(1)	(2)	(3)	(4)	(5)	(6)	(7)	(8)
SE	22.7(F)	1.28(F)	4.40(F)	0.11±0.05	1.57(7)	17.2±1.0 (40%)	12.5±0.8 (54%)
SE1	22.7(F)	1.28(F)	4.40(F)	0.11(F)	1.64(5)	6.05±0.6 (18%)	3.83±0.3 (28%)
SE2	22.7(F)	1.28(F)	4.40(F)	0.13±0.04	0.87(6)	6.87±0.6 (37%)	4.95±0.4 (52%)
SE3	22.7(F)	1.28(F)	4.40(F)	0.11±0.07	1.19(3)	4.48±0.7 (62%)	3.73±0.6 (75%)

4.3. Discussion - The hard component

One possibility as to the origin of the hard residual component, as alluded to (though not explicitly stated) in the previous sections, is that it could be due to the ‘wing’ emission from the very bright central source. This idea is supported by the fact that the spectrum of the hard residual emission (both the NW emission and the hard component of the SE emission) appears very consistent with the IC 4329A spectrum.

To investigate this question further, a radial surface brightness profile (over the channel range 11 to 235) of the central emission was formed. This is shown in Fig. 14 (with the region between 2.4′ and 12.6′ magnified in the inset), and contains many features, as follows: Firstly, the data points show the radial distribution (centered on IC 4329A) of the total X-ray emission, split into 21″ radial bins, with the region inside 1′ split into 7″ radial bins. The long dashed line represents the PSF of a point source with a spectrum best fitted by a power law of photon index 1.28, absorbed by a column of 2.27×10^{21} cm $^{-2}$, i.e. it represents the radial distribution of the emission from IC 4329A, assuming it to be a point source. This was formed by summing together model PSFs (for photons of varying energies), each normalized according to the spectrum of IC 4329A (i.e. normalized according to Fig. 7). The dotted line indicates the radial distribution of the true (i.e. non-diffuse) background. This was formed by firstly eliminating from an image all of the sources to very large radii ($5 \times$ the FWHM of the PSF). This resulted in an image where approximately none of the unresolved, extended emission, visible in Fig. 9, was included. A polynomial fit was then used to interpolate across the ‘holes’, and the image was then heavily smoothed (with a Gaussian of FWHM 9.4′). A radial profile of this image (again centered on IC 4329A) gives the indicated dotted line. The dash-dotted line indicates the level of the ‘diffuse’ emission, the unresolved emission visible in Fig. 9. This was formed by removing sources from an image to radii of twice the FWHM of the PSF. A mask image

was created in the same way with zero values at the positions of these holes, and values of unity everywhere else. A radial profile (of binsize 36″) was formed from the source subtracted image, and this was normalized for the area lost in the ‘holes’, by dividing it by an equivalent profile of the mask image.

Several features are evident within this figure. The central bright point source is very obvious, but also visible are the two other bright sources, the IC 4329 source (H5-P6), at $\approx 3'$, and H1-P3, at $\approx 13.5'$. The emission is seen to fall to the background level at large radii (9–18′), but there is a very notable deviation from this level closer in. Between 4′ and 9′ (and possibly up to 11′), the emission is seen to be significantly enhanced with respect to the background, and there appears to be two components to this enhancement. One is the presence of some underlying, unresolved, perhaps truly diffuse emission, as indicated by the dash-dotted line. The second is the presence of point sources, notably the bright sources P6, P9 and P16, visible in the radial profile figure, between 4.5′ and 6.5′, as data points lying above the residual emission profile. Part (or perhaps all) of the enhancement at $\approx 10'$ is due to sources P3 and P4.

With regard to the unresolved emission therefore, it is the dash-dotted, unresolved emission profile, and the possible contribution to this from the dashed IC 4329A point source that are of interest. It can be seen from Fig. 14 that the idealised point source model of IC 4329A does contribute to the unresolved emission within the inner annulus (NW1 & SE1: 2.25′–5′), though beyond this, in the outlying regions, the expected contribution drops rather quickly. The fact that the X-ray source associated with IC 4329A may not be an idealised point source however, as is suggested by Fig. 14, where some deviation from the (spectrally corrected) point source PSF model can be seen, may boost the true wing contribution in the outlying regions from this source, to values perhaps in line with that of the residual emission.

Perhaps therefore, the hard residual emission is due to the wings of IC 4329A. The hard residual emission is well fit by

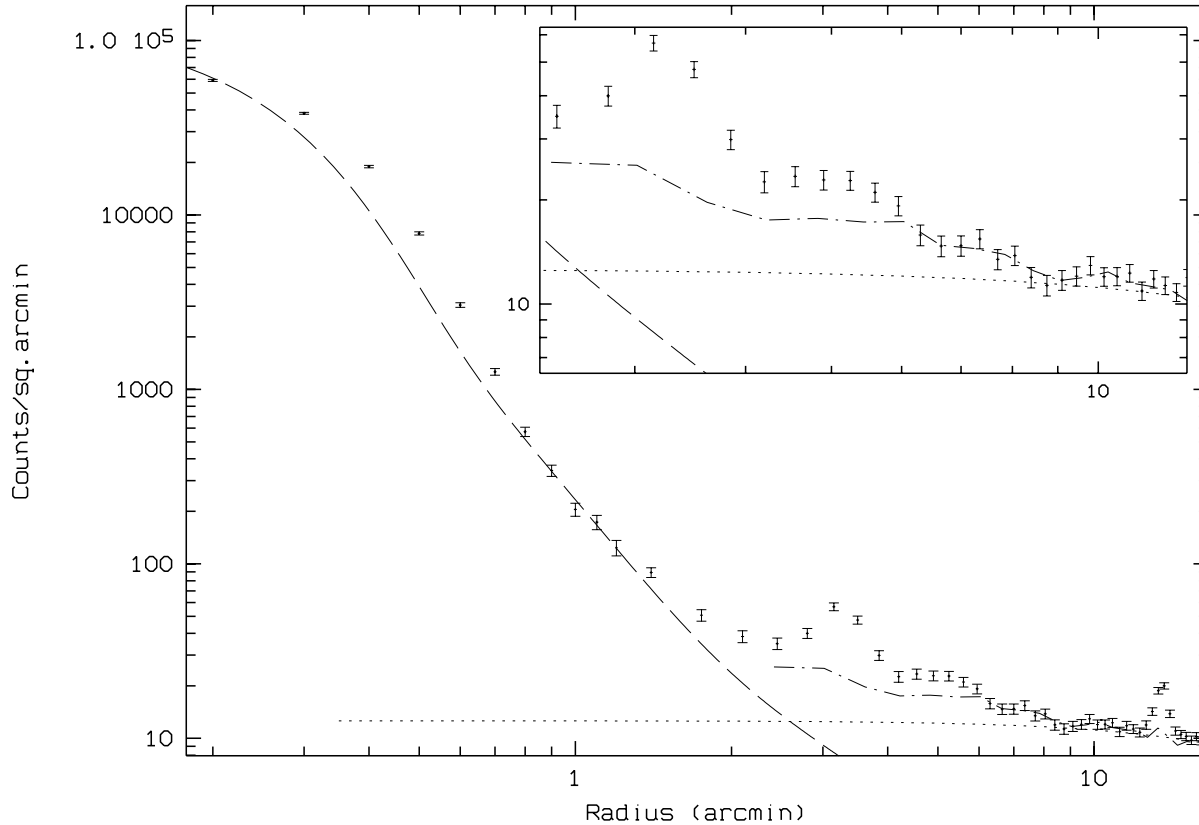


Fig. 14. Surface brightness profile of the (0.1–2.4 keV) flux about the centre of IC 4329A (the region between 2.4' and 12.6' is magnified in the inset). Data points show the total X-ray emission profile, the long dashed line represents the PSF of a point source with spectral properties identical to that of IC 4329A, the dash-dotted line indicates the level of the 'diffuse' emission, all point source emission having been removed, and the dashed line indicates the level of the 'true' background, all point source and 'diffuse' emission having been removed (see text).

the IC 4329A spectrum, and the number of counts expected from the IC 4329A wings may be close to being in agreement with what is observed (though this is unlikely). Furthermore, the hard residual emission appears approximately circular, and both smooth and regular, as one would expect, if this emission were just due to the wings of a bright point source. Unfortunately, there is one aspect of the hard residual X-ray emission that is very difficult to reconcile with it being due to the IC 4329A wings – the emission is *not* centred on IC 4329A. Instead, it appears centred on a point midway between IC 4329A and its bright elliptical companion, IC 4329, a point coincident with the 'bridge' of X-ray emission visible in the HRI data (Fig. 11). This fact, that the emission is not centred on IC 4329A, makes it very unlikely that the hard residual emission is due entirely to the IC 4329A wings.

Instead, the above points are very suggestive of the emission being due partly to the 'wings' of IC 4329A, and partly to hot gas surrounding the IC 4329A/IC 4329 pair. A significant fraction of the hard residual emission will be due to the IC 4329A wings, but this only makes a marked contribution at smaller radii, dropping to a level below half that of the total hard residual emission beyond $\approx 4'$. The fact that the spectral properties of the hard residual emission appear indistinguishable from those of IC 4329A may at first seem strangely coincidental.

In fact, this is not too surprising as the spectral capabilities of the ROSAT PSPC are not too good for harder spectra, and, to the PSPC, an IC 4329A-type spectrum and a hot (5–10 keV) plasma spectrum appear almost identical, as is apparent in the spectral fitting results (Table 5).

Nevertheless, we have attempted to further analyse the north-western unresolved emission spectra, in an attempt to extract any information regarding the hot gas component that may exist. A two-component model, comprising of a power-law component, representing the emission from the IC 4329A 'wings', and a Raymond and Smith hot plasma component, representing the diffuse hot gas component, was fitted to the full NW spectrum and to the three sub-spectra NW1, NW2 and NW3. Here, the power-law component parameters were frozen at the IC 4329A values ($N_H = 22.7 \times 10^{20} \text{ cm}^{-2}$, $\Gamma = 1.28$), and the Raymond & Smith component absorption column was frozen at the Galactic value ($4.4 \times 10^{20} \text{ cm}^{-2}$). Examination of the resultant Raymond & Smith component normalization-temperature parameter space reveals a similar effect in all but one of the cases; In the fits to the full NW spectrum, and to the inner NW1 and the outer NW3 spectrum, the temperature of the hot gas component is seen to be very ill-defined, with large, and highly irregularly-shaped confidence contour levels. Furthermore, no significant improvements in the fit quality are seen, reduced χ^2 s

(and number of degrees of freedom) for these three fits being: NW 0.86(9), NW1 0.63(5) NW3 0.30(3) (compare these values with the one-component Raymond and Smith values given in Table 5).

In the case of the NW2 spectrum however, a significant improvement is seen in the fit quality (reduced χ^2 (n.d.o.f) = 0.82(7) – compare with Table 5). Also the hot gas component normalization-temperature parameter space is seen to be quite well-defined, with (at least at the 68% confidence level) reasonably small and regularly-shaped contour levels (see Fig. 15). The best fit to the NW2 spectrum (indicated by the dot in Fig. 15) contains a IC 4329A-like component and a hot gas component with a temperature of $1.53_{-0.55}^{+4.35}$ keV.

We believe that we are only able to see this hot gas component, even reasonably, within the NW2 fit, because it is only at this radial distance from the central bright source that the contamination from the IC 4329A ‘wings’ drops sufficiently enough to allow the hot-gas component (which is itself dropping with radius) to become visible. In the NW1 spectrum, although the hot gas component is large, the IC 4329A wing component is huge, and the contamination is too large to allow a reasonable determination of the hot gas component parameters. In the NW3 spectrum, even though the IC 4329A wing component has become extremely low, the hot gas component is now very low itself, and the statistics involved are insufficient for a reasonable spectral determination.

A great range in temperature is able to fit the hot gas component of the full NW spectrum. We assume here though, that the temperature of the entire hot gas component is equal to the temperature found for the NW2 spectrum ($1.53_{-0.55}^{+4.35}$ keV). Fitting of the full NW spectrum, assuming this temperature, does lead to a very good fit indeed, with a reduced χ^2 of 0.52 (with 10 degrees of freedom).

Mean physical properties for this north-western hot gas can be inferred from the above results if we make some assumptions about the geometry of the emission. Here we have assumed the simple geometry of the north-western hot gaseous emission being hemispherical with a radius of 11.7' (in actuality, only a rough approximation to the gas properties can be calculated here and assumption of a slightly different radius gives rise to very similar results).

Using the volume derived for this hemispherical ‘bubble’ model, the fitted emission measure $\eta n_e^2 V$ (where η is the ‘filling factor’ – the fraction of the total volume V which is occupied by the emitting gas) can be used to infer the mean electron density, n_e , and hence the total mass M_{gas} , thermal energy E_{th} and cooling time t_{cool} of the gas.

Performing these calculations, after first accounting for the extra emission lost in the ‘holes’ left after the source-subtraction procedure, one arrives at approximate values to the physical properties of the north-western hot gaseous emission as follows; X-ray luminosity L_X (0.1–2.4 keV; intrinsic) 2.6×10^{41} erg s^{-1} ; n_e , $1.8 \times 10^{-4} \eta^{-0.5}$ cm^{-3} ; M_{gas} , $9.5 \times 10^{10} \eta^{0.5} M_{\odot}$; E_{th} , $8.1 \times 10^{59} \eta^{0.5}$ erg; t_{cool} , 99 Gyr. In the later discussion, we will see that no spectral information regarding the hot gaseous emission to the south-east can be obtained. This is primarily because

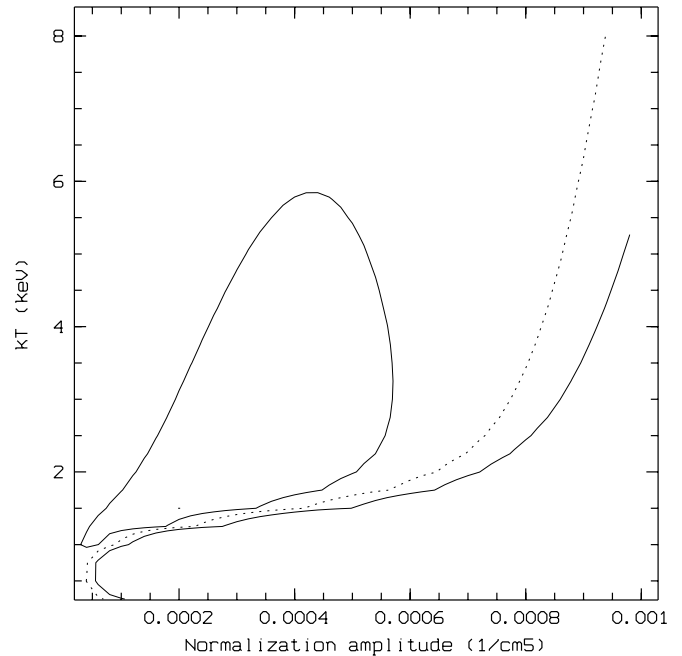


Fig. 15. Two-component model spectrum fit to the NW2 (middle) spectrum. Gaussian contour levels of 1σ , 2σ and 3σ in the hot gas (Raymond & Smith) component temperature–normalization plane for the (IC 4329A-like) power-law plus Raymond & Smith plasma fit to the NW2 spectrum (see text).

of this emission being severely contaminated, not only, as it is to the north-west, by the IC 4329A ‘wings’, but also by the very soft emission discussed earlier. If one makes the simple assumption that the properties of the hot gas to the south-east are identical to those to the north-west, a quite valid assumption, given the physical appearance of the emission and the level of accuracy we can attain, then the values of the physical properties for the total hot gas surrounding the IC 4329A/IC 4329 system become double those quoted above (except for the mean electron density n_e , and the cooling time t_{cool} , which remain unchanged).

Remembering that, as discussed in the introduction, the two central galaxies lie close to cluster A3574, and are part of a loosish group of seven galaxies, it is useful to compare here the properties of this hot gaseous emission component with the general X-ray properties of groups and clusters.

As regards the comparison with clusters, though the temperature of the hot gas may be comparable, the luminosity (5.2×10^{41} erg s^{-1}) is extremely low. Clusters typically have X-ray luminosities greater than 5×10^{43} erg s^{-1} (Edge & Stewart 1991; Yamashita 1992; White 1996), i.e. two orders of magnitude greater than is observed around IC 4329A/IC 4329, and it is therefore very unlikely that we are seeing emission associated with the A3574 cluster. In the following discussion, we will primarily deal with the comparison of the present results with the properties of galaxy groups.

The general X-ray properties of galaxy groups have recently been published, both of Hickson’s (1982) compact groups

(HCGs) (Ponman et al. 1996), and of other, poor groups (Mulchaey et al. 1995). The group containing IC 4329A and IC 4329 appears rather loose and contains perhaps seven members (a rather large number). A good optical image of the group can be found in Fricke & Kollatschny (1996).

The X-ray luminosity of the hot gaseous emission is low, but in no way uncomfortably low when compared to the results of Ponman et al. (1996) and Mulchaey et al. (1995). Many other galaxy groups at the same distance are seen with very similar hot gas X-ray luminosities (i.e. the emission from the member galaxies having been removed, as has been done here). Furthermore, the ratio of the diffuse hot gas X-ray luminosity to the total blue luminosity of the member galaxies L_X/L_B ($\approx 1.2 \times 10^{-3}$) is seen to be very typical of groups. As regards how the X-ray luminosity relates to the spiral fraction (the fraction of the group member galaxies that are spiral, as opposed to elliptical galaxies), the hot gas around IC 4329A/IC4329 is again, in no way unusual. The spiral fraction of the IC 4329A group is actually very high, IC 4329 being the only non-spiral member, and though Ponman et al. (1996) find only a very weak correlation between spiral fraction and L_X , Mulchaey et al. (1995) find a somewhat stronger correlation, all of the groups they detect having an extended X-ray emitting intragroup medium having a high percentage of early-type galaxies. The emission within the IC 4329A group (a high spiral fraction group) is of a low luminosity, in agreement with the work of Mulchaey et al. (1995) (and of Ponman et al. (1996) though only a far weaker correlation is seen here).

As regards the temperature of this hot gas however the emission may be unusual. As discussed earlier, it has proved very difficult to separate this emission from the wings of the bright central source associated with IC 4329A, and a good deal of caution should be taken here. Indeed, the present case is very similar to the case of HGC 4, as, while Saracco & Ciliegi (1995) suggest the existence of an extended component, Pildis et al. (1995) find that it is impossible to detect any extended diffuse component on account of the emission from the central active galaxy in the group being so strong.

Our tentative value though, for the temperature of the hot gas (≈ 1.5 keV) appears to be high when compared to the values of Ponman et al. (1996), which range, in the majority of cases, from 0.6–1 keV, and also when compared to the values of Mulchaey et al. (1995). Though a large error on the temperature does exist (see Fig. 15), it does appear that the temperature is constrained to be greater than 1 keV. The hot gaseous emission seen surrounding the IC 4329A/IC 4329 pair appears therefore, to be quite hot when compared to typical groups, and as such, it sits rather uncomfortably on the L_X –temperature relationship of Ponman et al. (1996), being of too low a luminosity for its temperature (or too hot for its L_X).

For rich clusters of galaxies (Edge & Stewart 1991), there appears to be a good correlation between L_X and the optical velocity dispersion σ . Extending the Edge & Stewart (1991) cluster relationship down, one would expect, in the case of groups, the higher velocity dispersion systems to have higher X-ray luminosities, and indeed, this does appear to be the case (Ponman et

al. 1996; Mulchaey et al. 1995); higher- σ groups are brighter in X-rays. The IC 4329A group of galaxies has a rather large value of σ , approximately 390 km s^{-1} , calculated using the Galaxy-corrected recession velocities given in the Third Reference Catalogue of Bright Galaxies (RC3; de Vaucouleurs et al. 1991). This value is greater (though within the range of) Hickson et al.'s (1992) study of 100 HCGs, which have a median value of 200 km s^{-1} . It is also larger than typical values for loose groups (208 km s^{-1} Geller & Huchra 1983; 183 km s^{-1} Maia et al. 1989), though much less than for rich clusters, where, for example, Zabludoff et al. (1990) established a median σ for 65 Abell clusters, of 744 km s^{-1} . Interestingly, there is good indication of a correlation between σ and the group emission temperature (Ponman et al. 1996), a correlation which appears to extend from the poorest of groups to the richest of clusters. IC 4329A, on account of its high temperature *and* its high velocity dispersion, lies directly on Ponman et al.'s (1996) $\sigma - T$ regression line, between the groups and the clusters. The hot gaseous emission within the IC 4329A group however, is not as X-ray luminous as the group's velocity dispersion would imply, and it lies below the regression line fitted to the $L_X - \sigma$ data of Ponman et al. (1996). It should be stressed however, that it does lie well within the scatter of the data, and cannot be called in any way, unusual.

In terms of the amount of gas present, the IC 4329A group appears again, quite normal. Its estimated gas mass of $\sim 2 \times 10^{11} M_\odot$ is very typical of groups (Mulchaey et al. 1995), lying on the low side of average, but well within the scatter.

In summary then, part of the emission detected surrounding IC 4329A and IC 4329, and extending out to two other galaxies in the group, IC 4327 and NGC 5298, may well be hot gaseous emission associated with the galaxy group. If it is, then the estimated temperature of the hot gas ($\gtrsim 1$ keV, quite hot for groups) agrees well with the (high) velocity dispersion of the group galaxies. Its X-ray luminosity however, appears to be lower than average (for its velocity dispersion and/or temperature). Similarly, the mass of gas involved is perhaps lower than average. In no way though, do any of the physical properties of the emission indicate that this IC 4329A group emission is very unusual.

Interestingly, the single galaxy group in Ponman et al.'s (1996) survey most similar to the IC 4329A group is HCG 48. This group has a high velocity dispersion as well, and a correspondingly high temperature (≈ 1.1 keV) is found for the hot gas. It's X-ray luminosity however, is low, and it is seen to lie significantly below the L_X -temperature relationship of Ponman et al. (1996), as do the present IC 4329A group results. Importantly, like the IC 4329A group, HCG 48 itself lies within a larger cluster, A1060, and it appears to be falling into this cluster. It may well be the case that we are seeing in both cases, the HCG 48 case and the IC 4329A case, the effects of gas stripping from these groups, as they fall through their respective clusters centres. This reduction in hot group gas would have the effect of reducing the observed L_X (and estimated gas mass), as is observed.

4.4. Discussion - The soft component

The soft residual component reveals itself in several different ways. It can be seen in the soft band (Ch. 8–41) image of Fig. 3, where the emission to the south-east of the central bright IC 4329A source is seen to be significantly enhanced with respect to the emission to the north-west. The most striking depiction of the residual soft component however, is in Fig. 10, where the adaptively filtered soft band image shows what appears to be a roughly semi-circular distribution of diffuse emission, ‘centred’ on IC 4329A, and extending out, though almost entirely to the south-east, to a radius of perhaps $10'$, past the two outlying sources H2/4-P4 and H16-P12. As seen, the spectral properties of this emission indicate that it is very likely to be due to a very low temperature (~ 0.1 keV) plasma, absorbed by a column consistent with that out of our Galaxy.

What is this soft emission then? One question that needs to be addressed first is, is this feature actually associated with IC 4329A? Perhaps it is a foreground feature. Perhaps it is very local, within our own Galaxy, or even within our local bubble. The spectral information present in the PSPC data is very useful here, as in Fig. 13, where the 1σ , 2σ and 3σ Gaussian contour levels in the soft-component temperature-absorption column parameter space are shown, it can be seen that this component’s spectrum appears to be best fit with a plasma spectrum with an absorption column equal to, or greater than, the column out of the Galaxy, i.e. the feature is very likely to be extragalactic, if no intrinsic absorption is present, a likely fact, given the amorphous, diffuse nature of the feature. The feature therefore, appears likely to be extragalactic. Is it associated with IC 4329A though? A couple of points regarding the structure of the feature are very suggestive, we believe, of this being the case. Firstly, a good correlation is seen between this soft feature and the disc of IC 4329A. Secondly, within this feature, a large plume of emission is visible lying directly perpendicular to the IC 4329A disc, to the south-east (see Fig. 10), i.e. along the galaxy’s minor axis. This plume is in the same direction as the 2.3 GHz radio feature discovered by Blank & Norris (1994). Furthermore, the HRI image (Fig. 11) shows good evidence for an extension in this south-eastern direction also. Lastly, the soft feature, although lying almost exclusively to the south-east of IC 4329A, is very symmetric with respect to the minor axis of IC 4329A, i.e. the level of emission seen to the north-east of the plume discussed above appears very similar to that to the south-west.

Assuming therefore, that the emission is connected in some way to the IC 4329A/IC 4329 system, then the fact that it is soft and intrinsically, almost completely unabsorbed, is very reminiscent of the galactic winds seen within the halos of many different systems (notably starburst systems) (Watson et al. 1984; Fabbiano 1988; Pietsch 1992; Strickland et al. 1997; Read et al. 1997). Indeed, many multi-wavelength studies of this system indicate that a wind is possibly present (see Sect. 1). Both Colbert et al. (1996) and Mulchaey et al. (1996) detect $H\alpha$ + $[NII]$ features extending along the minor axis, to $\sim 10''$ (3 kpc) on both sides of the nucleus, and both sets of authors believe that these features represent an outflow from the nucleus similar to

the superwinds commonly seen in edge-on infrared-luminous galaxies (e.g. McCarthy et al. 1987; Armus et al. 1990).

There are however, many differences between this feature and the ‘classic’ winds seen in such nearby starburst systems as M82 and NGC 253. Firstly, the feature is very large, extending to a radius of perhaps $10'$, which at the assumed distance of 64 Mpc, corresponds to a size of almost 200 kpc. This is over an order of magnitude greater than the classic features mentioned above. Secondly, it appears almost entirely on one side only of the system, to the south-east, and thirdly, it is rather luminous when compared to the classic starburst winds.

As for the hot gaseous emission in the previous section, mean physical properties for this cool, soft-component SE gas can be inferred, if we make some assumptions about the geometry of the emission. We could consider the emission to be in the form of a hemisphere, purely in the south-eastern direction. This is physically unreasonable however, and upon closer inspection, the best simple estimate for the geometry of the soft residual emission appears to be a sphere, centred to the south of IC 4329A, with a radius of $\approx 8'$ (150 kpc at the assumed distance of 64 Mpc). Again, only a rough approximation to the gas properties can be calculated here and assumption of either model gives rise to very similar results.

Using the volume derived for this spherical ‘bubble’ model, the fitted emission measure $\eta n_e^2 V$ can again be used to infer the mean electron density, n_e , the total mass M_{gas} , the thermal energy E_{th} and the cooling time t_{cool} of the gas, as follows; X-ray luminosity L_X (0.1–2.4 keV; intrinsic) 8.7×10^{41} erg s $^{-1}$; n_e , $3.4 \times 10^{-4} \eta^{-0.5}$ cm $^{-3}$; M_{gas} , $1.1 \times 10^{11} \eta^{0.5} M_{\odot}$; E_{th} , $7.0 \times 10^{58} \eta^{0.5}$ erg; t_{cool} , 2.6 Gyr.

Comparison of these values with values obtained for the soft extended features seen in several nearby spiral systems (including the ‘classic’ winds in NGC 253, M82, NGC 3079 and NGC 3628 (Read et al. 1997)), leads to the conclusion that the soft emission seen here, to the south-east of NGC 4329A, is even more unusual than at first thought. Not only, as mentioned above, is it much larger and brighter (both by at least an order of magnitude) and observed on only one side of the system, but it appears to be far less dense (again by over an order of magnitude), and extremely massive (perhaps a hundred times more so than for the NGC 253/M82 features). One must be careful here though, as a factor of $\sqrt{\eta}$ is still involved in the above results, and this could have quite a large effect on the results.

The soft feature seen here therefore, appears to be completely unlike the classic starburst winds (except in terms of the temperature, which appears to be consistent with the classic wind temperatures (Read et al. 1997). What this feature bears much more of a resemblance to, are the features seen associated with the ultraluminous far-infrared galaxies (FIRGs) Arp 220, NGC 2623 (Read & Ponman 1997) and NGC 6240 (Fricke & Papaderos 1996). Here, large, soft, outlying features are seen to one side, and one side only, of these high-luminosity systems, systems believed to be at the most energetic stage in the evolution of a merger between two galaxies, i.e. at the point where the nuclei of the two galaxies merge. However, the features seen in these systems, though more similar to the IC 4329A feature than

the ‘classic’ wind features, are, in some respects, still rather different. Though they are spectrally soft ($kT \lesssim 0.5$ keV), and large ($\lesssim 50$ kpc), much larger than the ‘classic’ wind features, they are still significantly smaller than the IC 4329A feature. Furthermore, though they are far brighter than the ‘classic’ wind features, they still have luminosities perhaps an order of magnitude smaller than the IC 4329A feature. It must be borne in mind here though that, as mentioned previously, IC 4329A is a superluminous Seyfert galaxy, with an X-ray luminosity some two orders of magnitude greater than that of Arp 220 (Read & Ponman 1997). In this respect, the IC 4329A ‘wind’ feature makes up a far smaller fraction of the total X-ray luminosity than in any of the FIRGs or starbursts.

The most striking similarity between the IC 4329A soft feature, and the FIRG soft features however, is perhaps the strangest facet of their emission – their one-sided nature. Why does the structure seen in IC 4329A appear only on one side of the system? As regards the FIRGs, and as is discussed in Read & Ponman (1997), the answer may lie in the fact that these systems are rapidly evolving. MacLow & McCray (1988) numerically modelled the growth of superbubbles: large thin shells of cold gas surrounding a hot pressurized interior, - essentially a galactic wind, or at least, the progenitor of, in various stratified atmospheres. They discovered that superbubbles blow out of the HI layer (i.e. they depart from the ‘snowplow’ phase and evolve into the ‘blowout’ phase), and are then able to move out into the inter-galactic medium at velocities of several thousand km s^{-1} (see Heckman et al. 1993). This, MacLow & McCray (1988) find, occurs when the superbubbles have a radius of between one and two scaleheights. What they also find however, is that these bubbles will blow out on *one side only* of a disc galaxy if the bubble centres are more than 50–60 pc from the centre of the disc of the galaxy. Now, in a (relatively) non-evolving system, such as M82 or NGC 253, the starburst is seen to be very symmetrically positioned with respect to the galactic disc, and bipolar structures are seen in the X-ray (Watson et al. 1984; Fabbiano 1988; Pietsch 1992; Strickland et al. 1997; Read et al. 1997). As discussed in Read & Ponman (1997) though, in the rapidly-evolving ultraluminous merging systems Arp220 and NGC 2623, the central burst is highly unlikely to be so centrally positioned with respect to the quickly-moving and highly distorted gaseous components, and the direction of steepest pressure gradient (along which the bubble will most rapidly expand) will now no longer be along both directions of the disc’s minor axis (as is the case in M82-type systems), but will be in just one direction (as is predicted by MacLow & McCray 1988), hence the observed one-sided blowout.

In the present case, it appears unambiguous that some sort of interaction between IC 4329A and IC 4329 is taking place: Both galaxies are close together and are part of a looser group of seven galaxies. IC 4329 appears to be a shell galaxy, a signature of interaction. Photographic co-addition and contrast enhancement of four UKST IIIa-J survey plates indicate the presence of low surface brightness features around IC 4329A (Wolstencroft et al. 1995), again suggestive of an interaction. Evidence for possible interaction-induced activity is also seen, as discussed earlier, in

the $H\alpha + [\text{NII}]$ studies of Colbert et al. (1996) and Mulchaey et al. (1996), and in the radio studies of Unger et al. (1987) and Blank & Norris (1994). Good evidence for an interaction is present also in the ROSAT HRI data. As seen previously, Fig. 11 shows what appears to be a ‘bridge’ of emission connecting the two galaxies. This type of feature is believed to have been seen in several different situations, though importantly, always in association with galaxies in the process of interacting. For instance, a near-identical feature is seen between the pair of interacting galaxies, NGC 3395/6 (Read & Ponman 1997), and at the contact region between the two galaxies making up the *Antennae* system (Read & Ponman 1995). Furthermore, a similar feature is seen within the galaxy group HCG 92 (Stefan’s Quintet) (Pietsch et al. 1997). It is thought probable that all of these features, including the present HRI feature between IC 4329A and IC 4329, are due to shocks resulting from strong galaxy interactions. So, though there is very strong evidence of an interaction occurring between IC 4329A and IC 4329, whether, as regards the above one-sided blowout discussion, this interaction is strong enough to displace the disc of IC 4329A with respect to the ‘central’ wind source, is unclear.

There is another possible explanation of this very soft emission related to the harder group emission discussed earlier. Remember that the high velocity dispersion of the IC 4329A group galaxies and the high fitted temperature to the X-ray emitting gas should point to the X-ray emitting gas having a high luminosity. This is observed however, not to be the case, and it was suggested that ‘stripping’ of some of the group gas as the group moves through the surrounding A3574 cluster medium may be taking place. This would result in a reduction in the X-ray luminosity and estimated mass of the group gas, as we see. As discussed earlier, this idea is given some credence by the fact that HCG 48, a group very similar to the IC 4329A group in terms of its high velocity dispersion and high X-ray temperature, combined with a low X-ray luminosity (Ponman et al. 1996), is also observed to be a group within a cluster (A1060), and is thought to be falling through the centre of the cluster.

Could this soft emission, seen to the south-east of the IC 4329A/IC 4329 pair, be this stripped group gas? The addition of the X-ray luminosity and gas mass of this soft component to the equivalent values for the harder ‘group’ component would certainly push the total group gas L_X and M_{gas} to values such that the entire properties of the IC 4329A group, taken as a whole, would appear completely normal and typical. As mentioned in the introduction, this group lies at the easternmost edge of the Hydra-Centaurus supercluster. Though no tangential velocities for these galaxies are obviously available, it could perhaps be safe to assume that the IC 4329A group would be moving tangentially in a general westward direction, towards the centre of this superstructure. Any gas stripped from this group would appear to the east of the group, as is observed in the case of the very soft emission.

Whether the temperature of this soft gas is consistent with this idea, is difficult to say. One might have expected any stripped gas to be harder than its equivalent group emission, though it might be possible that compression has led to cooling. In fact,

the (roughly) estimated cooling time of this gas is fairly short (less than 3 Gyr).

This idea, though interesting, may not be correct however, as perhaps the same morphology should be seen in the case of the hard group emission. Though this hard emission is severely contaminated by the IC 4329A wings, it does appear, on account of the fact that the total hard emission is centred some way between IC 4329A and IC 4329, that the hard group emission lies more predominantly to the opposite side of IC 4329A than the soft emission.

5. Summary

We have observed both the ROSAT HRI and PSPC data from fields centred on the edge-on, type 1 Seyfert galaxy IC 4329A and its nearby companion, the giant lenticular IC 4329. 17 and 22 sources are detected respectively in the full HRI and PSPC fields of view, the brightest being associated with the two central galaxies and a further source to the south-west. Many coincidences are seen in the two datasets and the nine most significant HRI sources all have equivalent PSPC counterparts. In addition to point source emission, unresolved residual emission is detected surrounding the IC 4329A/IC 4329 pair. This emission appears markedly two-component, with a smooth, circularly-distributed hard component, centred midway between the two central galaxies, and a more irregular, soft component, situated almost entirely to the south-east of IC 4329A. Our findings with regard to the observed point-source and unresolved emission can be summarized as follows:

1. An extremely bright ($L_X = 6 \times 10^{43} \text{ erg s}^{-1}$) source is detected associated with the central Seyfert IC 4329A. Its spectral properties are compatible with a single power-law ($\Gamma = 1.73$), with a spectral break at 0.7 keV, in very good agreement with previous authors' work.

2. Two other very bright sources are detected associated with the nearby giant lenticular IC 4329 ($L_X = 8 \times 10^{41} \text{ erg s}^{-1}$), and with a likely quasar to the south-west. Fitting of standard spectral models to these source spectra again result in fits that agree well with previous authors' work.

3. Many other bright sources are detected both in the HRI and PSPC fields of view, including three point-like sources, symmetrically positioned with respect to the disc of IC 4329A. Optical follow-up observations of these sources with the 2.2 m ESO/MPG telescope at La Silla, Chile, has established that they are nothing to do with the central Seyfert, being merely foreground and background objects.

4. None of the sources detected show any significant temporal variability.

5. In addition to the point sources, residual emission is detected, both in the HRI and in the PSPC, surrounding the IC 4329A/IC 4329 pair. This emission appears markedly two-component, comprising of a hard, smooth, circularly-distributed component, centred somewhere between IC 4329A and IC 4329, and a soft, irregular component, situated almost entirely to the south-east of the IC 4329A disc.

6. The hard component of the residual emission appears itself to be made up of two components. One of these is purely the 'wings' of the extremely bright IC 4329A source, visible out to several arcminutes. The second component appears to be hot ($\sim 1.5 \text{ keV}$) diffuse gas, with a luminosity of $\approx 5 \times 10^{41} \text{ erg s}^{-1}$ and a mass of perhaps $2 \times 10^{11} M_\odot$. The properties of this emission are very suggestive of it being due to hot gas within the galaxy group of which IC 4329A and IC 4329 are members.

7. The soft component of the residual emission, in terms of its temperature and one-sided nature, bears a good deal of resemblance to proposed starburst driven winds seen in some far-infrared ultraluminous systems. It is however much brighter ($L_X = 9 \times 10^{41} \text{ erg s}^{-1}$), and larger. Another possibility discussed briefly, is that the soft emission may be a 'wake' of stripped gas from the galaxy group.

8. A 'bridge-like' feature is detected with the HRI between the two central galaxies, and is likely, as is seen in other similar systems, to be due to shocks resulting from the strong interaction taking place between the two systems.

Acknowledgements. AMR acknowledges the grateful receipt of a Royal Society fellowship during this work. We are also very grateful to Andreas Vogler for his X-ray-optical overlay routines and to Trevor Ponman for useful discussions. This research has made use of the SIMBAD database operated at CDS, Strasbourg.

Optical images are based on photographic data obtained with the UK Schmidt Telescope, operated by the Royal Observatory Edinburgh, and funded by the UK Science and Engineering Research Council, until June 1988, and thereafter by the Anglo-Australian Observatory. Original plate material is copyright (c) the Royal Observatory Edinburgh and the Anglo-Australian Observatory. The plates were processed into the present compressed digital form with their permission. The Digitized Sky Survey was produced at the Space Telescope Science Institute under US Government grant NAG W-2166.

Finally, we thank our colleagues from the MPE ROSAT group for their support. The ROSAT project is supported by the German Bundesministerium für Bildung, Wissenschaft, Forschung und Technologie (BMBF/DARA) and the Max-Planck-Gesellschaft (MPG).

References

- Armus L., Heckman T.M., Miley G.K., 1990, ApJ 364, 471
 Baum S.A., O'Dea C.P., Dallacassa D., de Bruyn A.G., Pedlar A., 1993, ApJ 419, 553
 Blank D.L., Norris R.P., 1994, in Bicknell G.V. et al., eds, ASP Conf. Ser. Vol. 54, The First Stromlo Symposium: The Physics of Active Galaxies. Astron. Soc. Pac., San Francisco, p. 307
 Branduardi-Raymont G., et al., 1994, MNRAS 270, 947
 Cappi M., Mihara T., Matsuoka M., Hayashida K., Weaver K., Otani C., 1996, ApJ 458, 149
 Chincarini G., Rood H.J., 1979, ApJ 230, 648
 Colbert E.J.M., Baum S.A., Gallimore J.F., O'Dea C.P., Lehnert M.D., Tsvetanov Z.I., Mulchaey J.S., Caganoff S., 1996, ApJS 105, 75
 Cooke B.A., et al., 1978, MNRAS 182, 489
 Cruddace R.G., Hasinger G.R., Schmitt J.H.M.M., 1988, in Murtagh F., Heck A. (eds), Astronomy from large databases, ESO Conference and Workshop Proc. 28, p. 177
 Delvaile J.P., Geller M.J., Schnopper H.W., 1978, ApJ 226, L69

- de Vaucouleurs G., de Vaucouleurs A., Corwin H.G., 1964, Reference Catalogue of Bright Galaxies, University of Texas, Austin
- de Vaucouleurs G., de Vaucouleurs A., Corwin H.G., Jr., Buta R.J., Paturel G., Fouqué P., 1991, Third Reference Catalogue of Bright Galaxies (RC3). Springer-Verlag, New York
- Dickey J.M., Lockman F.J., *ARA&A* 28, 215
- Edge A.C., Stewart G.C., 1991, *MNRAS* 252, 428
- Fabbiano G., 1988, *ApJ* 330, 672
- Fabbiano G., Kim D.-W., Trinchieri G., 1992, *ApJS* 80, 531
- Fabian A.C., Nandra K., Celotti A., Rees M.J., Grove J.E., Johnson W.N., 1993, *ApJ* 416, L57
- Fiore F., Perola G.C., Matsuoka M., Yamauchi M., Piro L., 1992, *A&A* 262, 37
- Fricke K.J., Papaderos P., 1996 in Zimmermann H.-U., Trümper J.E., Yorke H. (eds), *Röntgenstrahlung from the Universe*, MPE report 263, p. 377
- Geller M.J., Huchra J.P.E., 1983, *ApJS* 52, 61
- Hasinger G., Turner T.J., George I.M., Boese G., 1992, OGIP calibration memo CAL/ROS/92-001
- Heckman T.M., Lehnert M.D., Armus L., 1993, in Shull J.M., Thronson H.A., eds, *The Environment and Evolution of Galaxies*, Kluwer Academic Publishers
- Hickson P., 1982, *ApJ* 255, 382
- Hickson P., Mendes de Oliveira C., Huchra J.P., Palumbo G.G.C., 1992, *ApJ* 399, 353
- Irwin M., Maddox S., McMahon R., 1994, *Spectrum*, 2, 14
- Jacoby G.H., Hunter D.A., Christian C.A., 1984, *ApJS* 56, 257
- Klemola A.R., 1969, *AJ* 74, 804
- Kollatschny W., Fricke K.J., 1989, *A&A* 219, 34
- Loewenstein M., Mushotzky R.F., Tamura T., Ikebe Y., Makishima K., Matsushita K., Matsumoto H., 1994, *ApJ* 436, L75
- MacLow M.-M., McCray R., 1988, *ApJ* 324, 776
- Madejski G.M., et al., 1995, *ApJ* 438, 672 (M95)
- Maia M.A.G., da Costa L.N., Latham D.W., 1989, *ApJS* 69, 809
- Matsushita K., et al., 1994, *ApJ* 436, L41
- McCarthy P., Heckman T.M., van Breugel W., 1987, *AJ* 93, 264
- Miyoshi S., Yamashita K., Okumura Y., Hayakawa S., Kunieda H., Nagase F., Tawara Y., 1988, *PASJ* 40, 127
- Mulchaey J.S., Davis D.S., Mushotzky R.F., Burstein D., 1995, *ApJ* 456, 80
- Mulchaey J.S., Wilson A.S., Tsvetanov Z., 1996, *ApJS* 102, 309
- Mushotzky R.F., 1984, *Adv. Space Res.* 3, No. 10, 157
- Mushotzky R.F., Fabian A.C., Iwasawa K., Kunieda H., Matsuoka M., Nandra K., Tanaka Y., 1995, *MNRAS* 272, L9
- Osterbrock D.E., 1991, *Reports on Progress in Physics* 54, 579
- Penston M.V., Wilson A.S., 1979, *ApJ* 232, 389
- Petre R., Mushotzky R.F., Krolik J.H., Holt S.S., 1984, *ApJ* 280, 499
- Pfeffermann E., et al., 1986, *Proc. SPIE* 733, 519
- Pietsch W., 1992, in Thuan T.X., Balkowski C., Thanh Van J.T., eds, *Physics of Nearby Galaxies: Nature or Nurture?* Editions Frontières, Gif-sur-Yvette, p. 76
- Pietsch W., Vogler A., Kahabka P., Jain A., Klein U., 1994, *A&A* 284, 386
- Pietsch W., Trinchieri G., Arp H., Sulentic J.W., 1997, *A&A* 322, 89
- Pietsch W., Bischoff K., Boller Th., et al., 1998, *A&A*, in press
- Pildis R.A., Bregman J.N., Evrard A.E., 1995, *ApJ* 443, 514
- Pincinotti G., Mushotzky R.F., Boldt E.A., Holt S.S., Marshall F.E., Serlemitsos P.J., Shafer R.A., 1982, *ApJ* 253, 485
- Piro L., Yamauchi M., Matsuoka M., 1990, *ApJ* 360, L35
- Ponman T.J., Bourner P.D.J., Ebeling H., Böhringer H., *MNRAS* 283, 690
- Rangarajan F.V.N., Fabian A.C., Forman W.R., Jones C., 1995, *MNRAS* 272, 665
- Raymond J.C., Smith B.W., 1977, *ApJS* 35, 419
- Read A.M., Ponman T.J., Wolstencroft R.D., 1995, *MNRAS* 277, 297
- Read A.M., Ponman T.J., Strickland D.K., 1997, *MNRAS* 286, 626
- Read A.M., Ponman T.J., 1997, submitted to *MNRAS*
- Roche N., Shanks T., Georgantopoulos I., Stewart G.C., Boyle B.J., Griffiths R.E., 1995, *MNRAS* 273, L15
- Rush B., Malkan M., Fink H.H., Voges W., 1996, *ApJ* 471, 190
- Saracco P., Ciliegi P., 1995, *A&A* 301, 348
- Saslaw W.C., Valtonen M.J., Aarseth S.J., 1974, *ApJ* 190, 253
- Shapley H., 1936, *Harvard Bull.* 903, 17
- Snowden S.L., McCammon D., Burrows D., Mendenhall J., 1994, *ApJ* 424, 714
- Strickland D.K., Ponman T.J., Stevens I.R., 1997, *A&A* 320, 378
- Tanaka Y., et al., 1984, *PASJ* 36, 641
- Tennant A.F., Mushotzky R.F., 1983, *ApJ* 264, 92
- Trümper J., 1992, *QJRAS* 33, 165
- Unewisse A., 1993, PhD thesis, University of Sydney, Sydney, New South Wales, Australia
- Unger S.W., Lawrence A., Wilson A.S., Elvis M., Wright A.E., 1987, *MNRAS* 228, 521
- Watson M.G., Stanger V., Griffiths R.E., 1984, *ApJ* 286, 144
- White D.A., 1996, in Zimmermann H.-U., Trümper J.E., Yorke H. (eds), *Röntgenstrahlung from the Universe*, MPE report 263, p. 621
- Winkler H., Glass I.S., van Wyk F., Marang F., Spencer-Jones J.H., Buckley D.A.H., Sekiguchi K., 1992, *MNRAS* 257, 659
- Wolstencroft R.D., Done C.J., Scarrott S.M., Scarrott R.M.J., 1995, *MNRAS* 276, 460
- Yamashita K., 1992 in Tanaka Y., Koyama K. (eds), *Frontiers of X-ray Astronomy*. Universal Academy Press, Tokyo
- Zabludoff A.I., Huchra J.P., Geller M.J., 1990, *ApJS* 74, 1
- Zdziarski A.A., Lightman A.P., Maciolek-Niedzwiecki A., 1993, *ApJ*, 414, L93
- Zimmermann H.-U., Belloni T., Boese G., et al., 1992, in Guyenne T.D., Hunt J.J. (eds), *Proc. European ISY conference*, ESA ISY-3, p. 231
- Zimmermann H.-U. et al., 1994, *EXSAS User Guide*, 4th edition